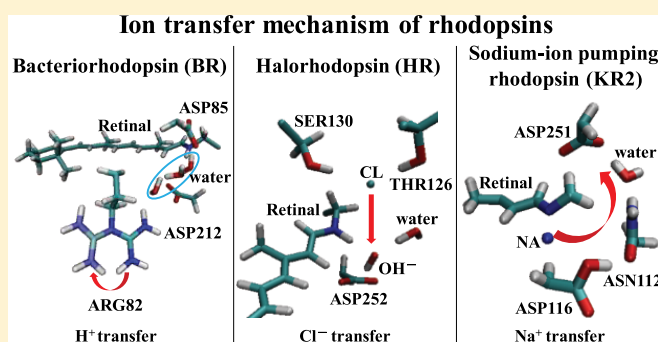


# Light-Driven Proton, Sodium Ion, and Chloride Ion Transfer Mechanisms in Rhodopsins: SAC-CI Study

Tomoo Miyahara\*<sup>1</sup> and Hiroshi Nakatsuji\*<sup>2</sup>

Quantum Chemistry Research Institute, Kyoto Technoscience Center 16, 14 Yoshida Kawara-machi, Sakyou-ku, Kyoto 606-8305, Japan

## Supporting Information



**ABSTRACT:** Bacteriorhodopsin (BR) and halorhodopsin (HR) are well-known light-driven ion-pumping rhodopsins. BR transfers a proton from the intracellular medium to the extracellular medium. HR takes in chloride ion from the extracellular medium. A new light-driven sodium ion-pumping rhodopsin was discovered in 2013 by Inoue, Kandori, and co-workers (*Nat. Commun.* 2013, 4, 1678). The purpose of this article is to elucidate the proton, sodium ion and chloride ion transfer mechanisms and the geometrical changes of the intermediates. The absorption maxima of three rhodopsins were calculated by the SAC/SAC-CI method using the QM/MM optimized geometries. For BR, the SAC-CI results supported the previously proposed proton-transfer mechanism; (1) the photoisomerization from all-trans to 13-cis retinal (K intermediate), (2) the relaxation of the retinal structure (L intermediate), (3) the proton transfer from the Schiff base to the counterion residue (ASP85) (M intermediate), (4) the proton transfer from the ASP96 to the Schiff base (N intermediate), and (5) the thermal isomerization from 13-cis to all-trans retinal (O intermediate). The proton releases to the extracellular medium through the ASP96, the Schiff base, the ASP85, and the GLU204 or GLU194 from the intracellular medium. Furthermore, it clarified that the guanidine group rotation of ARG82 changes the excitation energies of the L and N intermediates, but the effect is small for the resting state and the K, M, and O intermediates. The theoretical calculations suggested that the ARG82 rotation occurs in the N intermediate from the comparison between the experimental absorption spectra and the theoretical excitation energies. For the KR2, the Kandori group proposed the sodium ion transfer mechanism; (1) the photoisomerization from all-trans to 13-cis retinal (K intermediate), (2) the relaxation of the retinal structure (L intermediate), (3) the proton transfer from the Schiff base to the counterion residue (ASP116) (M intermediate), (4) the sodium ion passes through the cavity formed by the rotation of the counterion residue (ASP116) (O intermediate) and (5) the proton of the ASP116 reassociates to the Schiff base. The steps (1) to (3) are the same as ones of BR. The SAC-CI results supported the proposed sodium ion transfer mechanism and suggested that the sodium ion transfer proceeds in the O intermediate as follows; (1) the sodium ion connects with the Schiff base in the cavity formed by the ASP116 rotation, (2) at the same time that the sodium ion passes through the Schiff base, the Schiff base forms the hydrogen bond to the proton of ASP116, and (3) at the same time that the sodium ion transfers to the extracellular medium, the proton reassociates with the Schiff base from the ASP116. Furthermore, our results indicated that the retinal is not all-trans but 13-cis when the sodium ion passes through the Schiff base in the O intermediate. For the HR, since the counterion residue is replaced by the THR126, the proton does not transfer from the Schiff base. Instead, the chloride ion transfers in the opposite direction to the proton of BR and the sodium ion of KR2. The SAC-CI results supported the previously proposed chloride ion transfer mechanism; (1) the photoisomerization from all-trans to 13-cis retinal (K intermediate), (2) the relaxation of the retinal structure (L intermediate), (3) the chloride ion passes through the Schiff base from the extracellular medium side to the intracellular medium side (N intermediate) and (4) the chloride ion transfer from the Schiff base to the intracellular medium and the thermal isomerization from 13-cis to all-trans retinal (O intermediate). Furthermore, our results suggested that the Schiff base forms bonds to the hydroxide ion instead of the chloride ion in the O intermediate. The negative ion is necessary to keep the total charge around the Schiff base in the O intermediate.

## 1. INTRODUCTION

Bacteriorhodopsin (BR)<sup>1,2</sup> and halorhodopsin (HR)<sup>3,4</sup> that are the light-driven ion-pumping rhodopsins were discovered in 1970s. The BR transfers a proton from the intracellular medium to the extracellular medium and the HR transfers chloride ion in

Received: October 19, 2018

Revised: February 8, 2019

Published: February 14, 2019

the opposite direction to the BR. Furthermore, sensory rhodopsins (SR)<sup>5,6</sup> and channel rhodopsins (ChR)<sup>7,8</sup> were also discovered. The SR converts a light to a signal by binding to transducer protein and the ChR functions as a light-gated ion channel. In 2013, a sodium ion pumping rhodopsin (KR2: *Krokinobacter eikastus* rhodopsin 2) was discovered by Inoue, Kandori and others.<sup>9</sup> Since these light-driven rhodopsins are found in Archaea, Bacteria, and Eukaryota, they are commonly called microbial rhodopsins. It is common to the microbial rhodopsins that the functions are induced by the photoisomerization of the retinal chromophore from all-trans to 13-cis.

Since these discoveries of BR and HR, the structures, mechanisms and functions of microbial rhodopsins have been studied by many researches.<sup>10–22</sup> In BR, the photocycle and the protonated state of retinal of each state are shown in Figure 1. The excitation energies of the ground states of the resting state and five intermediates (K, L, M, N, and O) are shown in wavelength (nm) and energy (eV).<sup>23</sup> The resting state has all-trans retinal and its absorption maximum is observed at 568 nm (2.18 eV). The photoexcitation leads the transition to the red-shifted K intermediate ( $\lambda_{\text{max}} = 610$  nm) due to the isomerization from all-trans to 13-cis retinal. No photon is needed in the reaction after the K intermediate. The K intermediate changes to the blue-shifted L intermediate ( $\lambda_{\text{max}} = 550$  nm) by the

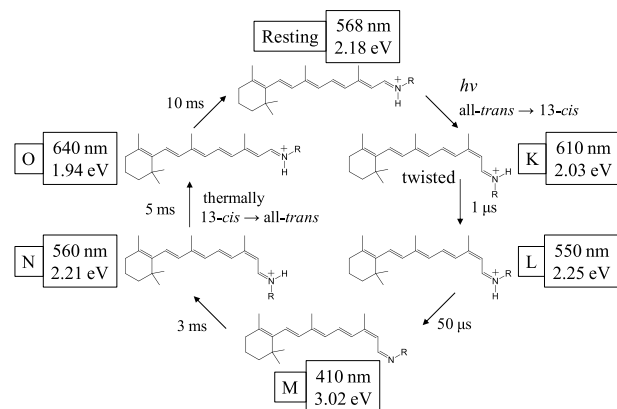


**Figure 1.** Photocycle of bacteriorhodopsin (BR). The resting state and the O intermediate have the all-trans retinal. The K, L, M, and N intermediates have the 13-cis retinal. The Schiff base deprotonates for the M intermediate. The retinal changes to the 15-syn conformation in the L intermediate and returns to the 15-anti conformation in the N intermediate. Absorption maximum of each state is shown in wavelength (nm) and energy (eV).<sup>23</sup> Time scale is referred to ref 37.

relaxation of the twisted retinal in about 1  $\mu$ s. Next, the proton transfers to aspartic acid (counterion residue; ASP85) from the Schiff base. This proton transfer forms the M intermediate ( $\lambda_{\text{max}} = 410$  nm) with a large blue-shifted absorption of the retinal. The N intermediate ( $\lambda_{\text{max}} = 560$  nm) is formed by two proton transfers: one is the proton release to the extracellular medium from the proton-releasing complex (GLU194 and GLU204), and the other is the reprotonation to the Schiff base from the proton donor ASP96. The proton-releasing complex and ASP96 are shown in Figure 2. The red-shifted O intermediate ( $\lambda_{\text{max}} = 640$  nm) is formed by the proton transfer to ASP96 from the intracellular medium and by the thermal isomerization to all-trans retinal. Finally, the BR returns to the resting state by the proton transfer from the ASP85 to the proton-releasing

complex. The photocycle from the photoisomerization to the M intermediate is fast due to the retinal structural relaxation and the short-range proton transfer. However, the processes after the M intermediate are slow due to the long-range proton transfer and the thermal isomerization of retinal.

In the sodium ion pumping rhodopsin (KR2), the photocycle and the protonation state of retinal shown in Figure 3 are very similar to those of BR. KR2 also has two aspartic acids (ASP116 and APSP251) shown in Figure 4 as in the case of BR. The

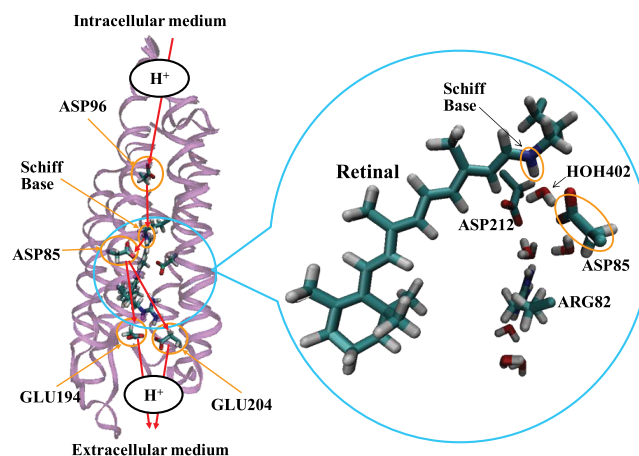


**Figure 2.** Geometry and proton transfer process of bacteriorhodopsin (BR) (PDB ID: 1C3W<sup>77</sup>). Three-dimensional structure of BR is shown as magenta. Carbon, hydrogen, oxygen and nitrogen atoms are shown as cyan, gray, red and blue, respectively. ASP, GLU, and ARG represent aspartic acid, glutamic acid, and arginine, respectively. Some water molecules (HOH) around the Schiff base and ARG82 are also shown. Orange circles represent the proton donor and acceptor sites. In the right, the retinal and its surrounding structures are rotated and enlarged from the configuration in the left. Red arrows represent the flow of proton transfer. (1) Proton transfers to ASP85 from Schiff base of retinal. (2) Proton releases to the extracellular from GLU194 or GLU204. (3) Proton transfers to Schiff base from ASP96. (4) Proton transfers to ASP96 from the intracellular. (5) Proton transfers to GLU194 or GLU204 from ASP85.

retinal changes into the 13-cis from the all-trans by the photoexcitation in the K intermediate and then the proton transfers to the counterion residue (ASP116; ASP85 in BR) in the M intermediate. However, in the M intermediate, the sodium ion cannot pass through the Schiff base due to the steric effect between the protonated ASP116 and the sodium ion. Therefore, Kandori group suggested the sodium ion transport mechanism;<sup>9,24,25</sup> the sodium ion transport pathway is produced due to the rotation of the protonated ASP116 that forms the hydrogen-bond to the ASN112. We call it the R intermediate in this article. The proton of the ASP116 reassociates with the Schiff base in the O intermediate after the sodium ion passes through the Schiff base. Recently, this mechanism was supported by the computational study by Suomivuori et al.<sup>26</sup> Furthermore, many researches were performed in order to elucidate the photocycle in the KR2.<sup>27–35</sup> However, in KR2, the structures, transfer processes and functions are not resolved especially in the O intermediate. We considered the possibility of both 13-cis ( $O_{\text{cis}}$ ) and all-trans ( $O_{\text{trans}}$ ) retinal in O intermediate in this article.

In halorhodopsin (HR), which is a chloride ion pumping rhodopsin discovered in 1970s,<sup>3,4</sup> the photocycle is very similar to that of the BR. However, the HR has no counterion residue,



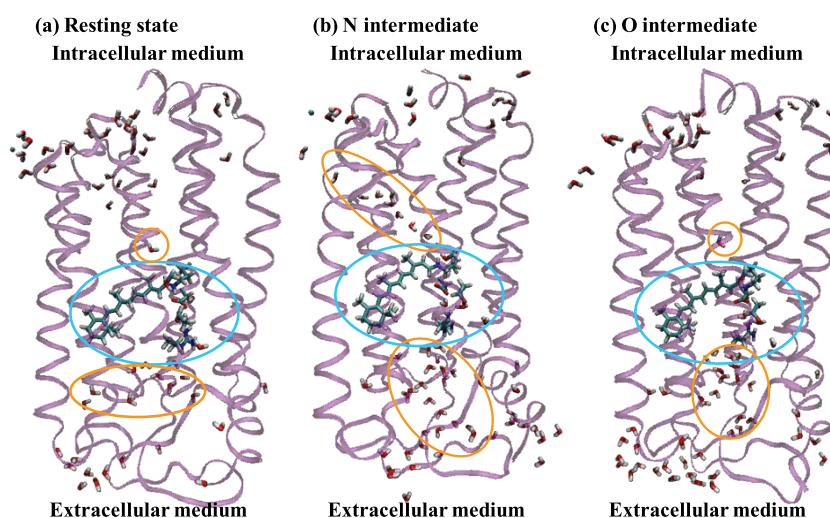


**Figure 7.** Geometries of the resting state (a), and the N (b) and O (c) intermediates of halorhodopsin (HR) (PDB ID: 3A7K,<sup>82</sup> 4QRY,<sup>39</sup> and 3QBG<sup>83</sup>). Three-dimensional structures of HR are shown as magenta. Carbon, hydrogen, oxygen, and nitrogen atoms are shown as cyan, gray, red, and blue, respectively. Light blue circle represent the retinal and its surrounding structures. Orange circles represent the water molecules around the retinal.

animal rhodopsins. A lot of research of microbial and animal rhodopsins was summarized in the review by Ernst and Kandori et al.<sup>37</sup>

Previously, we calculated the electronic structures of retinal and the interactions between the retinal and the opsin in four human visual pigments by using the symmetry adapted cluster-configuration interaction (SAC-CI) method<sup>41–44</sup> and clarified that the color-tuning is regulated by amino acids at specific positions as well as structural distortion of the retinal chromophore.<sup>45–49</sup> The SAC/SAC-CI theory was established for the ground and excited states of molecules<sup>41–44</sup> and has been applied to the world of the photochemistry and photo-biology.<sup>45–69</sup>

The SAC-CI method have successfully assigned the whole spectra of the photosynthetic reaction center (PSRC) of *Rhodospseudomonas viridis* and elucidated the mechanism of the electron transfer in the PSRC,<sup>55–61</sup> the excitation and emission of green fluorescent proteins,<sup>62,63</sup> the color-tuning mechanism of human vision,<sup>45–49</sup> the firefly luminescence mechanism,<sup>64</sup> the artificial color-tuning of firefly by the theoretical mutation<sup>65</sup> and the weak interactions of the double-helical structures of DNA and RNA.<sup>66–69</sup> Thus, the SAC-CI method is a powerful technique for photobiology. Recently, the time-dependent density functional theory (TD-DFT)<sup>70–72</sup> was used for the studies of the excited states. However, its results strongly depend on the functionals used.<sup>73–76</sup> To obtain the valuable information from the theoretical calculations, the accurate and reliable excited-state theory is necessary for the understanding of experiments. The SAC/SAC-CI method satisfies these requirements.

In this article, to clarify the ion-pumping mechanism of BR, KR2 and HR explained above, we have theoretically calculated the excited states of intermediates in the photocycle by the SAC/SAC-CI method. In BR, since the ARG82 around the Schiff base is surrounded by water molecules, the guanidine group ( $-C-(NH_2)_2^+$ ) can easily rotate. This rotation largely affects the excitation energy of BR by the change of the distance between the positive charge of ARG82 and the Schiff base. Therefore, we have also confirmed the relation between the excitation energies and geometrical changes around the Schiff base in each intermediate by the ARG82 rotation. In KR2, we

calculated two models ( $O_{cis}$  and  $O_{trans}$ ) to confirm whether the retinal is 13-cis or all-trans in the O intermediate where the sodium ion passes through the retinal Schiff base. In HR, since HR does not include a chloride ion inside the protein in the O intermediate, the total charge around the Schiff base is different between the O intermediate and other models. Therefore, we also calculated another two models for the O intermediate. One is the ARG123 rotation model; the guanidine group of the ARG123 rotates about 180 deg from the position of the X-ray crystallographic structure. The guanidine group rotation may change the excitation energy as explained in the section of BR. The other is the hydroxide ion model; the Schiff base forms the hydrogen bond to the HOH503 that is not water ( $H_2O$ ) but hydroxide ion ( $OH^-$ ). The hydroxide ion model keeps the total charge between the O intermediate and the other models. As explained below, in BR, the SAC-CI results showed that the ARG82 rotation has a large effect on the excitation energy for only the L and N in BR. In KR2, the SAC-CI results supported the sodium ion transfer mechanism proposed by Kandori group and suggested that the retinal is not all-trans but 13-cis when the sodium ion passes through the Schiff base. In HR, the SAC-CI results suggested that the HOH503 becomes hydroxide ion in the O intermediate. The single strong peaks are observed in the experimental absorption spectra of three rhodopsins. The wavelengths (excitation energies) of the peaks change during the photocycle of rhodopsin. The main configurations of all peaks are the excitation from the HOMO ( $\pi$  orbital) to LUMO ( $\pi^*$  orbital) with a strong oscillator strength. Therefore, we discuss the relation between the excitation energy of the HOMO–LUMO excitation and the geometry in each model of three rhodopsins in this article.

## 2. MODELING

**2.1. Bacteriorhodopsin (BR).** We showed the geometry and proton transfer process of the resting state of BR using the X-ray crystallographic structure (PDB ID:1C3W) in Figure 2. ASP, GLU and ARG represent aspartic acid, glutamic acid and arginine, respectively. Some water molecules (HOH) around the Schiff base and ARG82 are shown. Proton transfers in following five processes. (1) Proton transfers to ASP85 from Schiff base of retinal. (2) Proton releases to the extracellular

medium from GLU194 or GLU204. (3) Proton transfers to Schiff base from ASP96. (4) Proton transfers to ASP96 from the intracellular medium. (5) Proton transfers to GLU194 or GLU204 from ASP85. Thus, a proton transfers from the intracellular medium through ASP96, retinal Schiff base, ASP85, and GLU204 (or GLU194) to the extracellular medium. There are two aspartic acids (ASP85 and ASP212) around the retinal Schiff base. However, the proton transfers not to the ASP212 but to the ASP85 from the Schiff base. In the proton-releasing complex, there are two protonated sites of the GLU204 and GLU194. Either the GLU194 or the GLU204 receives the proton from the ASP85 and releases it to the extracellular medium. Both protonated sites are close to the extracellular medium and are situated to be about 13.5 Å from the Schiff base. Since the difference between two protonated states has little effect on the electronic states of the retinal Schiff base, we assumed that the GLU204 is the protonated site of the proton-releasing complex in this study.

We constructed initial geometries of the resting state and five intermediates (K, L, M, N, and O) based on the X-ray crystallographic structures.<sup>77–81</sup> Table 1 summarizes the protein data bank ID used in this article and the protonated states of three amino acids and the Schiff base.

The retinal Schiff base is protonated except for the M intermediate. In the resting state, the carboxylic acid is protonated for the ASP96 and GLU204 but deprotonated for the ASP85. The K and L intermediates have the same protonated sites as the resting state, because the proton transfer does not occur in these structural changes. In the M intermediate, the protonated ASP85 and deprotonated Schiff base are generated by the proton transfer from the Schiff base to the ASP85. The N intermediate is generated by two proton transfers from the ASP96 to the Schiff base and from the GLU204 to the extracellular medium. Therefore, in the N intermediate, the Schiff base and the ASP85 are protonated but the ASP96 and GLU204 are deprotonated. In the O

**Table 1. Protein Data Bank ID and Protonated Sites of Each Model of Bacteriorhodopsin**

model	PDB ID	ASP96 <sup>f</sup>	Schiff base <sup>f</sup>	ASP85 <sup>f</sup>	GLU204 <sup>f</sup>
resting	1C3W <sup>a</sup>	○	○	×	○
K	1MOK <sup>b</sup>	○	○	×	○
L	1O0A <sup>c</sup>	○	○	×	○
M	1P8H <sup>d</sup>	○	×	○	○
N	1P8U <sup>d</sup>	×	○	○	×
O	3VHZ <sup>e</sup>	○	○	○	×

<sup>a</sup>Reference 77. <sup>b</sup>Reference 78. <sup>c</sup>Reference 79. <sup>d</sup>Reference 80. <sup>e</sup>Reference 81. <sup>f</sup>○ and × represent “protonated” and “deprotonated”, respectively.

intermediate, the ASP96 receives the proton from the intracellular medium. Finally, the BR returns to the resting state by the proton transfer from the ASP85 to the GLU204.

The protonated guanidine group ( $-\text{C}-(\text{NH}_2)_2^+$ ) of the ARG82 can easily rotate due to the existence of water molecules as shown in Figure 2. Since the guanidine group of the ARG82 is situated to be about 8 Å from the Schiff base, the movement of the guanidine group with a positive charge affects the electronic states of retinal. Therefore, we calculated two models: one is the X-ray model taken from the X-ray crystallographic structure and the other is the rotation model in which the guanidine group of

the ARG82 rotates about 180 deg from the position of the X-ray crystallographic structure.

**2.2. Sodium Ion Pumping Rhodopsin (KR2).** We showed the geometry of KR2 in Figure 4. We calculated the resting state as well as the K, M, R, and O intermediates of KR2. The X-ray crystallographic structures (PDB ID: 3X3C)<sup>24</sup> was used for the initial geometry of the resting state of KR2. For the intermediate states (K, M, R, O) of KR2, we could not find the X-ray crystallographic structures. Therefore, referring to the optimized geometry of BR, the initial geometry of each intermediate was constructed by inserting the retinal structure of each intermediate into the QM/MM optimized geometry of the previous state of KR2. Just like with BR, the ARG109 rotation may increase the SAC-CI excitation energy as noted below. However, we did not consider the ARG109 rotation, because the excitation energies of KR2 were calculated to be higher than the experimental values in the SAC-CI calculations without the ARG rotation.

The first intermediate was obtained by the QM/MM geometry optimization of the K model whose initial geometry was composed of the retinal of the K intermediate of BR and the opsin of the resting state of KR2. The obtained retinal geometry is close to that of the K intermediate of BR. However, the SAC-CI value (2.29 eV) is closer to the experimental value (2.45 eV) of the L intermediate than that (2.05 eV) of the K intermediate. Therefore, we call it a KL model in this article. In the M model, the proton of the Schiff base moves to the ASP116. In the R model, the protonated ASP116 forms the hydrogen-bond to the ASN112 by the rotation of the carboxyl group of ASP116.

The sodium ion passes through the Schiff base in the O intermediate. First, the sodium ion bonds with the Schiff base. Second, the sodium ion passes through the Schiff base and moves to near the ASP251. Third, the ASP116 rotates and forms the hydrogen-bond to the Schiff base. Fourth, the proton moves to the Schiff base from the ASP116. The sodium ion transfers to the extracellular medium in the steps 3 or 4. When the sodium ion passes through the Schiff base, there are two possibilities that the retinal remains the 13-cis or isomerizes to the all-trans. Therefore, to elucidate the sodium ion transfer mechanism, we calculated the following models.

In the O<sub>cis</sub> model, the Schiff base bonds with the sodium ion that is transferred from the intracellular medium. After the sodium ion moved to near the ASP251, the protonated ASP116 still forms the hydrogen-bond to the ASN112 in the O1 model. In the O2 model, the protonated ASP116 forms the hydrogen-bond to the Schiff base. In the O3 model, the proton reassociates with the Schiff base from the ASP116 but the sodium ion exists near the ASP251. In the O4 model, the sodium ion is released to the extracellular medium. For the models O1 to O4, we prepared two models of the 13-cis (O<sub>cis</sub> model) and all-trans (O<sub>trans</sub> model) retinal. The O4'<sub>trans</sub> model is similar to the O4<sub>trans</sub> model, but the O2<sub>trans</sub> model is used as the initial geometry of the O4'<sub>trans</sub> model because the ASN112 rotates in the O3<sub>trans</sub> model. Therefore, we calculated ten models for the O intermediate. The positions of the sodium ion and the proton in each model are summarized in Table 2. From these calculations, we can elucidate the geometries in the O intermediate: whether the retinal is all-trans or 13-cis, whether or not the sodium ion bonds with the Schiff base and whether or not the proton reassociates with the Schiff base from the ASP116.

**2.3. Halorhodopsin (HR).** The geometry of HR is shown in Figure 6. BR has two aspartic acids around the Schiff base, but one aspartic acid of the counterion residue replaces to the

threonine for HR (THR126 in HR; ASP85 in BR). Therefore, the Schiff base is not deprotonated during the photocycle in HR. Instead, the chloride ion transfers to the intracellular medium from the extracellular medium. This is the opposite direction to the proton transfer in BR and the sodium ion transfer in KR2. In

**Table 2. Positions of Sodium Ion and Proton in the O Intermediate Model of KR2**

model	Na <sup>+</sup> <sup>a</sup>	H <sup>+</sup> <sup>b</sup>
O0 <sub>cis</sub>	○	ASP116
O1 <sub>cis</sub>	○	ASP116
O2 <sub>cis</sub>	○	ASP116
O3 <sub>cis</sub>	○	schiff base
O4 <sub>cis</sub>	×	schiff base
O1 <sub>trans</sub>	○	ASP116
O2 <sub>trans</sub>	○	ASP116
O3 <sub>trans</sub>	○	schiff base
O4 <sub>trans</sub>	×	schiff base
O4' <sub>trans</sub>	×	schiff base

<sup>a</sup>○ and × represent that Na<sup>+</sup> is included in the model or not, respectively. <sup>b</sup>Schiff base and ASP116 represent that H<sup>+</sup> bonds with the Schiff base and ASP116, respectively.

the resting state, the chloride ion (CL) is stable due to the hydrogen bonds by the Schiff base, SER130, THR126 and water molecules.

We calculated the resting state and the K, N and O intermediates of HR. The X-ray crystallographic structures (PDB ID: 3A7K,<sup>82</sup> 4QRY,<sup>39</sup> 3QBG<sup>83</sup>) was used for the initial geometry of the resting, N and O states. However, we could not find the X-ray crystallographic structure of the K intermediate. Therefore, referring to the optimized geometry of BR, the initial geometry was constructed by inserting the K intermediate retinal structure of BR into the QM/MM optimized geometry of the resting state of HR. For the K intermediate model, since the twisted structure around the retinal Schiff base was relaxed by the QM/MM optimization, the obtained retinal structure was close to the L intermediate of BR. Therefore, we call it a KL model in this article. For the KL model, we also calculated the KL<sub>Arg</sub> model in which the guanidine group of ARG123 rotates from that of the KL model. In the initial geometry of the N model, the chloride ion forms the hydrogen bond to the hydroxyl group of SER130 in the intracellular medium side of the Schiff base. For the O intermediate, we calculated three models of O<sub>Org</sub>, O<sub>Arg</sub> and O<sub>OH</sub>. In the O<sub>Org</sub> model, the initial geometry is taken from the X-ray crystallographic structure. In the O<sub>Arg</sub> model, the guanidine group of ARG123 rotates from the configuration of the O<sub>Org</sub> model. In the O<sub>OH</sub> model, the HOH503 that forms the hydrogen bond to the Schiff base becomes the hydroxide ion. The O<sub>OH</sub> model has the negative ion instead of the chloride ion, but the O<sub>Org</sub> and O<sub>Arg</sub> models have no negative ion instead of the chloride ion around the Schiff base.

### 3. COMPUTATIONAL DETAILS

In BR, the initial geometries were taken from the X-ray crystallographic structures listed in Table 1. In the KR2, the initial geometry of the resting state was taken from the X-ray crystallographic structures (PDB ID: 3X3C<sup>24</sup>). For the KL model of KR2, the initial geometry was constructed by inserting the retinal structure of the K intermediate of BR into the QM/MM optimized geometry of the resting state of KR2. For other models, the QM/MM optimized geometry of the previous

intermediate was used as an initial geometry except for the proton of the Schiff base, sodium ion and the rotation of ASP116. In the HR, the initial geometry of the resting, N and O states are taken from the X-ray crystallographic structures (PDB ID: 3A7K,<sup>82</sup> 4QRY,<sup>39</sup> 3QBG<sup>83</sup>). The initial geometry of the KL model of HR is constructed by inserting the K intermediate retinal structure of BR into the QM/MM optimized geometry of the resting state of HR just as in the case of the KR2.

The hydrogen atoms were attached to amino acids and water molecules by the TINKER software<sup>84</sup> using the AMBER99 force field<sup>85</sup> and to retinal by GaussView.<sup>86</sup> The geometry optimization of the whole protein was carried out using the QM/MM method.<sup>45–49</sup> The QM region includes the whole retinal chromophore with the side chain of LYS216 in BR (LYS255 in KR2 and LYS256 in HR) and the other atoms are included in the MM region. In the geometry optimized calculations, the density functional theory<sup>87</sup> with the B3LYP functional<sup>88,89</sup> was employed using the double- $\zeta$  plus polarization basis sets (6-31G(d))<sup>90</sup> for the QM region, and the AMBER99 force field<sup>85</sup> was used as a point charge for the MM region. The electrostatic potential of the MM region affects the retinal chromophore. All optimized geometries are given in PDB format in Supporting Information. Visual molecular dynamics (VMD)<sup>91</sup> is used for the visualization of the X-ray crystallographic structures and the optimized geometries.

The SAC-CI calculations were performed using the structures obtained by the QM/MM geometry optimized calculations in the Gaussian suite of program.<sup>92</sup> In the SAC-CI calculations, the QM region included the retinal chromophore, some amino acids and some water molecules that form the hydrogen-bonding network; ASP85, ASP212, and three water molecules in BR, ASP116, ASP251, ASN112, and one water molecule in KR2, ASP252, SER130, and two or three water molecules in HR. The sodium ion was included in the O models of KR2, and the chloride ion was included in the G, KL and N models of HR. Other amino acids (including the ARG82 in BR, ARG109 in KR2 ARG123 in HR) and other water molecules were included in the MM region. The double- $\zeta$  plus polarization basis sets (D95(d,p))<sup>93</sup> were used for the retinal  $\pi$ -conjugation system, the N and H atoms of the Schiff base, the chloride ion, the O and C atoms of the carboxylate groups of aspartic acid, and the water molecules. For the sodium ion, the double- $\zeta$  plus polarization basis sets were used.<sup>94</sup> Furthermore, a single p-type anion function ( $\alpha = 0.059$ )<sup>93</sup> was augmented on the O atoms of the ASP85 and ASP212. For the other atoms, the double- $\zeta$  basis sets (D95)<sup>93</sup> were used. In the SAC-CI calculations, all single and selected double excitations were included. Perturbation selection<sup>95</sup> was carried out with the threshold sets of LevelTwo. The core orbitals and the virtual orbitals whose energies were more than 3.0 au were treated as frozen core.

## 4. GEOMETRY AND PHOTOCYCLE OF BACTERIORHODOPSIN (BR)

**4.1. Excitation Energy.** The single strong absorption peaks are observed in the experimental spectra and the peak positions change during the photocycle of rhodopsin. The peaks correspond to the lowest excited state from the HOMO ( $\pi$  orbital) to LUMO ( $\pi^*$  orbital) with a strong oscillator strength. All excitation energies in this article indicate the HOMO–LUMO excitation.

The SAC-CI excitation energies of the X-ray and rotation models of BR are compared with the experimental values in Table 3. The retinal has the  $\beta$  ionone ring (left) and the Schiff

base (right) as shown in Figure 8a. Since the HOMO and LUMO are localized to the  $\beta$  ionone ring and the Schiff base, respectively, as shown in Figures 8, parts b and c, the excitation is the intramolecular electron transfer from the  $\beta$  ionone ring to the Schiff base. Therefore, the excitation energies of retinal of BR are affected by the electrostatic potential (ESP) change due to the rotation of the guanidine group of the ARG82.

For the X-ray models, the SAC-CI excitation energies were calculated to be lower than the experimental values except for the M intermediate model with the deprotonated Schiff base in the computational condition used in this article. Therefore, the deviations of the SAC-CI values from the experimental values

**Table 3. Excitation Energies of Bacteriorhodopsin (BR) (eV)**

state	SAC-CI		exptl <sup>a</sup>	$\Delta$	
	X-ray	rotation		X-ray	rotation
resting	2.11	2.15	2.18	-0.07	-0.03
K	1.78	1.78	2.03	-0.25	-0.25
L	2.05	2.27	2.25	-0.20	+0.02
M	3.14	3.18	3.02	+0.12	+0.16
N	1.79	2.01	2.21	-0.42	-0.20
O	1.69	1.70	1.94	-0.25	-0.24

<sup>a</sup>Reference 23.

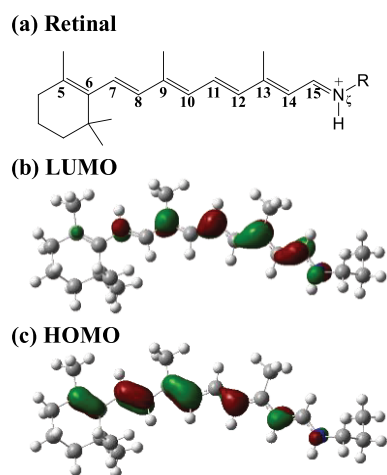


**Figure 8.** (a) Chemical formula of retinal. (b) LUMO and (c) HOMO of resting state of bacteriorhodopsin (BR).

may have relation to the protonation of the Schiff base. The SAC-CI values agreed with the experimental values within 0.25 eV except for the N intermediate model. However, for the N model, the excitation energy came to close to the experimental value by the rotation of the guanidine group. Therefore, for the N intermediate, the direction of the guanidine group may be different from that of the X-ray crystallographic structure under the measurement of the experimental absorption spectra.

In the rotation model, since the guanidine group moves away from the retinal Schiff base, its excitation energy becomes higher than that of the X-ray model. In particular, for the L and N models, the guanidine group rotation changes the excitation energy higher by about 0.2 eV. However, for the resting and M models, the excitation energy change is less than 0.1 eV. For the K and O models, the excitation energy remains unchanged by the guanidine group rotation. For the resting state and K, M, and

O intermediates, the effect of the guanidine group rotation is canceled by the rearrangement of the hydrogen-bonding network around the Schiff base as explained below.

**4.2. Resting State Model.** In the X-ray model of the resting state, the Schiff base forms the hydrogen bond to the HOH402 that forms the hydrogen bonds to the ASP85 and ASP212 as shown in Figure 9a. The ASP85 is also bound with the ASP212 by the hydrogen bonds through HOH401 and HOH406. Furthermore, the ARG82 forms the hydrogen bonds to three water molecules including the HOH406. Thus, the hydrogen-bonding network is formed between the Schiff base, ASP85, ASP212, and ARG82 through water molecules.

In the rotation model, the HOH403 rotates along with the guanidine group of the ARG82 and moves to the position of the HOH406 of the X-ray model as shown in Figure 9b. The ARG82 forms the hydrogen-bonding network with the ASP212 and ASP85 through the water molecules (HOH407, HOH403, and HOH406). However, the HOH401 is out of the hydrogen-bonding network. The guanidine group of ARG82 with a

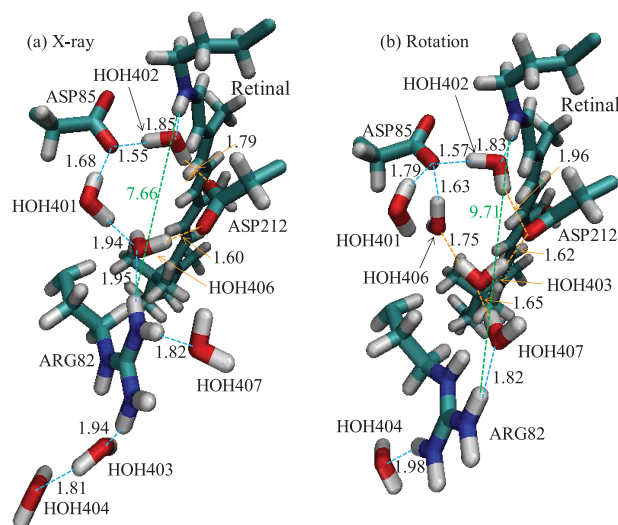


**Figure 9.** Optimized geometries of X-ray (a) and rotation (b) models of the resting state of BR.

positive charge is away from the Schiff base by 2.05 Å (7.66 Å to 9.71 Å). However, the HOH403 and HOH407 come close to the Schiff base by the rearrangement of the hydrogen-bonding network and the hydrogen atoms of HOH403 turn toward the Schiff base. Therefore, the excitation energy changes a little between the X-ray and rotation models, because the effect of the guanidine group rotation is canceled by the movement of two water molecules, HOH403 and HOH407.

**4.3. K Intermediate Model.** For the K intermediate models, the excitation energies are lower than those of the resting state due to the structural distortion of the retinal by the isomerization from the all-trans to the 13-cis. For the X-ray model in Figure 10a, the K intermediate forms the hydrogen-bonding network similar to that of the resting state. However, the Schiff base has no hydrogen bond and the arrangement of the HOH401 and HOH406 are different between the resting and K models.

In the rotation model, The ARG82 is separated from the hydrogen-bonding network formed by ASP85, ASP212, and three water molecules (HOH401, HOH402, and HOH406) as shown in Figure 10b. The guanidine group is away from the

Schiff base by 3.76 Å due to the rotation. However, the HOH406 comes close to the Schiff base and the hydrogen atoms of HOH401 and HOH406 turn toward the Schiff base in the rotation model. Therefore, the excitation energy remains unchanged between the X-ray and rotation models due to the

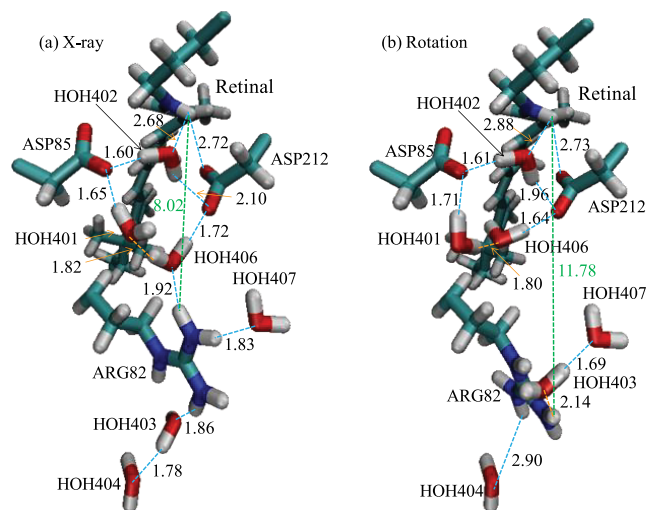


**Figure 10.** Optimized geometries of X-ray (a) and rotation (b) models of the K intermediate of BR.

cancellation of two effects: (1) the distance between the guanidine group and the Schiff base and (2) the directions and the positions of the hydrogen atoms of HOH401 and HOH406.

**4.4. L Intermediate Model.** In the L intermediate model, the distortion of retinal is reduced and the Schiff base forms the hydrogen bond to the HOH402 again as shown in Figure 11a. The direction of the hydrogen atom of the Schiff base seems to be different from that of the study by Kouyama et al.<sup>96</sup> In the study, the Schiff base forms the hydrogen-bond to the water molecule that exists in the intracellular medium side of the Schiff base. Therefore, the retinal has a 13-cis,15-anti conformation. However, we could not find any water molecules that forms the hydrogen-bond to the Schiff base in the intracellular medium side of the X-ray crystallographic structure used in this study. Therefore, the retinal has a 13-cis,15-syn conformation in the L intermediate model. The arrangement of water molecules (HOH401, HOH402, and HOH406) is similar to those of the resting and K models.

In the rotation model shown in Figure 11b, there is no water molecule that connects to the ARG82 with the ASP212 just like the K rotation model. The HOH401 is away from the Schiff base in the rotation model while keeping the hydrogen-bonding network. The distance between the guanidine group and the Schiff base increases from 7.31 to 10.94 Å. However, since the arrangement is similar between the X-ray and rotation models, the cancellation by the rearrangement of water molecules does not occur in the L model. Therefore, the excitation energy of the rotation model is higher than that of the X-ray model by 0.22 eV because of the guanidine group rotation.

**4.5. M Intermediate Model.** In the M intermediate models, since the proton moves from the Schiff base to the ASP85 through the HOH402, the excitation energy is higher than those of other models. This is corresponding to the large blue-shifted absorption observed in the experiment. In the X-ray model shown in Figure 12a, the hydrogen-bonding network around the

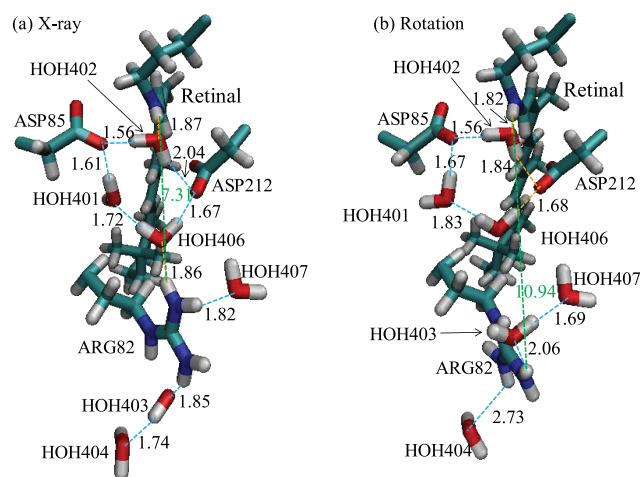


**Figure 11.** Optimized geometries of X-ray (a) and rotation (b) models of the L intermediate of BR.

Schiff base is similar to those of the resting and L models. The 13-cis, 15-syn retinal in the M model is different from the 13-cis, 15-anti conformation by the study of Kouyama et al.<sup>97</sup> as in the case of the L intermediate. The 15-syn/anti conformation may change easily by the experimental condition.

In the rotation model shown in Figure 12b, the ARG82 is separated from the hydrogen-bonding network of ASP85, ASP212 and water molecules just like those of the K and L models. For the M model, the guanidine group rotation does not change the arrangement of the water molecules around the Schiff base. This small geometrical change is different from those of the resting and K models. Although the positive charge of the guanidine group is away from the Schiff base by about 4 Å, the

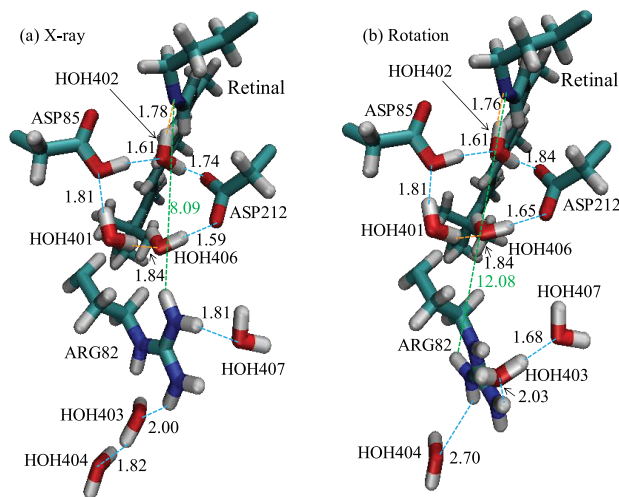


**Figure 12.** Optimized geometries of X-ray (a) and rotation (b) models of the M intermediate of BR.

excitation energy change is small, because the electrostatic potential (ESP) change at each atom of retinal is similar between the X-ray and rotation models as described later.

**4.6. N Intermediate Model.** In the N intermediate, the Schiff base receives the proton from the ASP96 on the intracellular medium side, and there is no water molecule that forms the hydrogen bond to the Schiff base in the extracellular

medium side. Therefore, the Schiff base forms the hydrogen bond to the water molecule in the intracellular medium side. In the X-ray model shown in Figure 13a, four water molecules form the hydrogen bonds to the guanidine group of the ARG82. However, in the rotation model, three of four water molecules are away from the guanidine group and form the hydrogen bonds to other amino acids.

In the rotation model shown in Figure 13b, the arrangements of the HOH401 and HOH406 are different from those of the X-ray model. The oxygen atom of the HOH401 turns to the Schiff base by the guanidine group rotation. Therefore, the movements of water molecules strengthen the effect of the guanidine group rotation. As a result, the excitation energy of the rotation model becomes higher than that of the X-ray model by 0.22 eV and comes close to the experimental value due to two effects; the guanidine group rotation and the HOH401 movement.

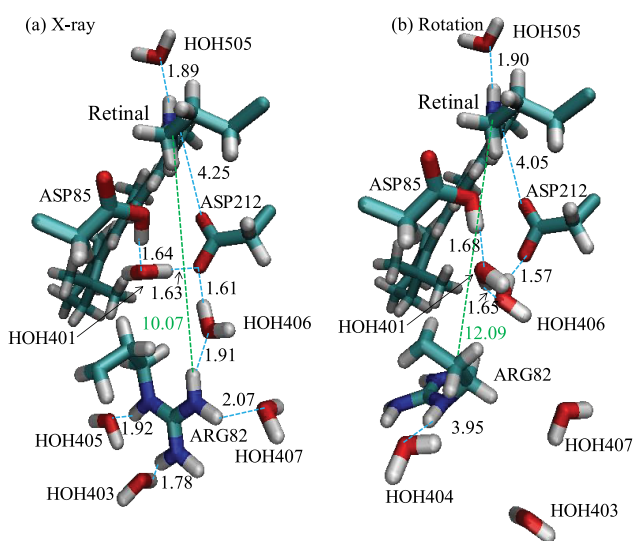


**Figure 13.** Optimized geometries of X-ray (a) and rotation (b) models of the N intermediate of BR.

**4.7. O Intermediate Model.** In the O intermediate, the Schiff base forms the hydrogen bond to the ASP212 instead of the water molecule (HOH602). In the X-ray model in Figure 14a, the HOH604 connects the ASP212 with the ARG82 through the hydrogen bonds. However, there is no hydrogen bond between the HOH603 and HOH604 unlike the resting, K, L, and M models.

In the rotation model in Figure 14b, the HOH604 forms the hydrogen bond to the HOH603 instead of the ARG82. The guanidine group is separated from the hydrogen-bonding network composed of ASP85, ASP212, and three water molecules (HOH602, HOH603, and HOH604). The geometry of the rotation model is similar to those of the K, L, and M models. The hydrogen atoms of the HOH602 and HOH603 turn to the Schiff base in the rotation model. Four water molecules exist around the ARG82 in the X-ray model but are away from the ARG82 in the rotation model. This geometrical change is similar to that of the N model. The excitation energy remains unchanged by the cancellation of the guanidine group rotation and the rearrangement of water molecules.

**4.8. ARG82 Rotation Effect.** The guanidine group rotation of the ARG82 affects the excitation energies of the L and N models, but the effect is small for the resting, K, M and O

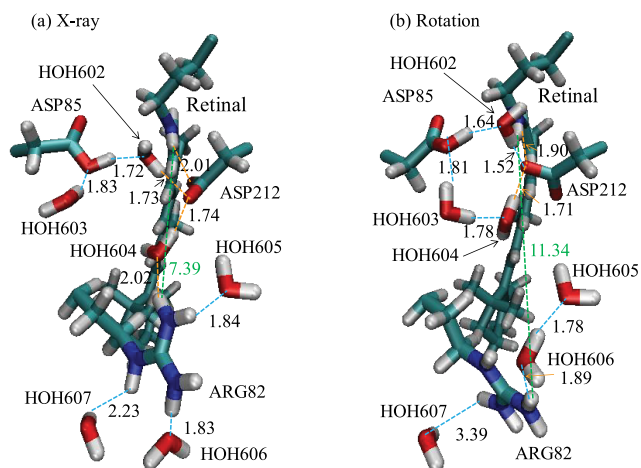


**Figure 14.** Optimized geometries of X-ray (a) and rotation (b) models of the O intermediate of BR.

models. The electrostatic potential (ESP) at each atom of retinal are shown in Figure 15. The ESP difference between the X-ray and rotation models is very small for the resting and the K intermediate models (Figure 15, parts a and b). Therefore, the excitation energy change between the X-ray and rotation models is small for the resting state and K intermediate. However, the ESP difference is large for the L, M, N, and O intermediates. The ESP of the rotation models decreases from the X-ray models at all atoms for the L and M intermediate models (Figures 15, parts c and d), at the C9 to N $\zeta$  for the N intermediate model (Figure 15e) and at the C5 to C13 for the O intermediate model (Figure 15f). When the N $\zeta$ -to-C5 difference in the ESP is large, the excitation energy is large because the HOMO–LUMO gap increases.<sup>49</sup> For the L and N intermediate models, the excitation energies increase by about 0.2 eV in the rotation model due to the increase of the N $\zeta$ -to-C5 difference in the ESP. However, for the O intermediate model, the N $\zeta$ -to-C5 difference in the ESP is very small, because the ESP decreases at the C5 to C13 but increases at the C14 to N $\zeta$ . Therefore, the excitation energy remains unchanged. For the M intermediate, the ESP difference at each atom is slightly large but the N $\zeta$ -to-C5 difference in the ESP is small. Therefore, the excitation energy change is small. As a result, the excitation energy largely changes only for the L and N intermediate models by the rotation of the guanidine group of the ARG82.

For the L and N intermediate models, the excitation energy of the rotation model is closer to the experimental value than that of the X-ray model. This shows a possibility that the guanidine group rotates from the X-ray structure under the measurement of the experimental absorption spectra. However, for the resting state and K, M and O intermediate models, since the excitation energy change is very small between the X-ray and rotation models, it is difficult to say whether or not the guanidine group rotates. If the guanidine group rotates only for the N intermediate, the deviation from the experimental value is within  $-0.25$  to  $-0.20$  eV for the K, L, N, and O intermediates with the protonated Schiff base with 13-cis retinal. Therefore, these data may suggest that the guanidine group rotates in only the N intermediate.

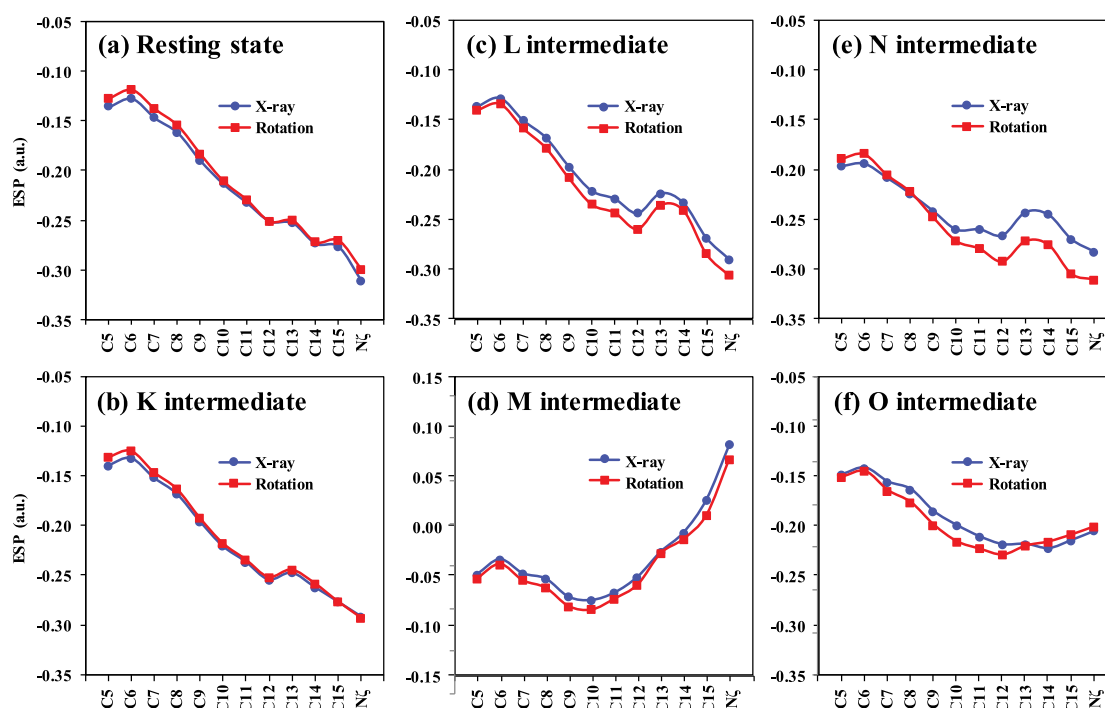


**Figure 15.** Electrostatic potential (ESP) at each atom of retinal in the X-ray and rotation models of the resting state (a) and K (b), L (c), M (d), N (e), and O (f) intermediates. Blue and red represent the ESP of the X-ray and rotation models, respectively.

## 5. GEOMETRY AND PHOTOCYCLE OF SODIUM ION PUMPING RHODOPSIN (KR2)

In Table 4, the SAC-CI excitation energies are compared with the experimental values<sup>9</sup> along with the distances between the sodium ion or the hydrogen atom of the carboxyl group of ASP116 and the nitrogen atom of the Schiff base. The optimized geometries around the Schiff base of the resting state and intermediate models are explained below.

**5.1. Resting State Model.** In the resting state, the proton of the Schiff base forms the hydrogen bonds to the carboxyl group of the ASP116 that forms the hydrogen bond to the ASN112 as shown in Figure 16a. The water molecule (HOH959) connects the ASN 112 with the ASP251 by the hydrogen bonds. Thus, the hydrogen-bonding network is formed around the Schiff base of retinal. The Schiff base directly connects to the ASP116 of the counterion residue for the KR2. This is major different from BR in which the Schiff base forms the hydrogen bond to the water molecule (HOH402 in Figure 9). The SAC-CI excitation energy (2.49 eV) agreed with the experimental value (2.36 eV) within 0.13 eV for the resting state. In the computational condition used in this article, the SAC-CI values seem to be slightly higher than the experimental values as shown in Table 4.

**5.2. KL Intermediate Model.** In the KL model, the retinal structure is close to the K intermediate model of bacteriorhodopsin (BR) by the QM/MM geometry optimization. The retinal has a 13-cis,15-anti conformation due to the hydrogen bond between the Schiff base and ASP116. In the experiment, the blue-shifted L intermediate (2.45 eV) as well as the red-shifted K intermediate (2.05 eV) was observed; the difference absorbance appears at around 605 nm (2.05 eV) in the transition absorbance spectra.<sup>9</sup> The SAC-CI values of KR2 are calculated to be higher than the experimental values in the computational conditions of this article (Table 4). The SAC-CI value (2.29 eV) of the KL model is higher than the experimental value (2.05 eV) of the K intermediate but is lower than the experimental value

**Table 4.** Excitation Energies and the Distances between Na<sup>+</sup> or H<sup>+</sup> of COOH of ASP116 and the Nitrogen Atom of the Schiff Base of KR2

model	excitation energy			distance	
	SAC-CI (eV)	exptl <sup>b</sup> (eV)	$\Delta$ (eV)	Na <sup>+</sup> -N <sup>c</sup> (Å)	H <sup>+</sup> -N <sup>d</sup> (Å)
resting	2.49	2.36	+0.13	—	—
KL	2.29	2.05 (K)	+0.24	—	—
		2.45 (L)	-0.16		
M	3.23	3.10	+0.13	—	1.80
R	3.36	—	—	—	4.19
O0 <sub>cis</sub>	2.46	2.19	+0.27	2.21	4.17
O1 <sub>cis</sub>	2.71	—	+0.52	2.71	3.84
O2 <sub>cis</sub>	2.56	—	+0.37	2.82	1.74
O3 <sub>cis</sub> <sup>a</sup>	1.42	—	-0.77	2.65	—
O4 <sub>cis</sub>	2.39	—	+0.20	—	—
O1 <sub>trans</sub>	2.95	—	+0.76	2.29	3.63
O2 <sub>trans</sub> <sup>a</sup>	2.74	—	+0.55	2.27	3.01
O3 <sub>trans</sub>	1.94	—	-0.25	2.58	—
O4 <sub>trans</sub>	2.85	—	+0.66	—	—
O4' <sub>trans</sub>	2.19	—	0.00	—	—

<sup>a</sup>Nonoptimized geometry is used. <sup>b</sup>Reference 9. L and K in parentheses represent the experimental values of the L and K intermediates. <sup>c</sup>Distance between Na<sup>+</sup> and the nitrogen atom of the Schiff base. <sup>d</sup>Distance between H<sup>+</sup> of COOH of ASP116 and the nitrogen atom of the Schiff base.

(2.45 eV) of the L intermediate. Furthermore, the SAC-CI value (2.29 eV) is lower than that (2.49 eV) of the resting model. This agrees with the relation between the K intermediate (2.05 eV) and the resting state (2.36 eV) in the experimental value. However, the experimental value (2.45 eV) of the L intermediate is higher than that of the resting state. Therefore, we concluded that the KL model corresponds to the K

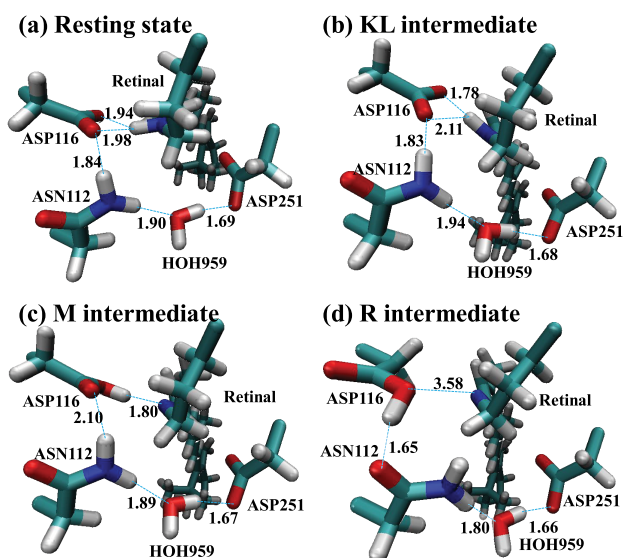


**Figure 16.** Optimized geometries of resting state (a), KL (b), M (c), and R (d) intermediate models of KR2.

intermediate due to its retinal structure as well as the comparison between the SAC-CI and experimental values.

In the KL model shown in Figure 16b, the hydrogen-bonding network is very similar to that of the resting state. The difference between the resting and KL models appears in the hydrogen-bonding distances between the ASP116 and the Schiff base. Two O atoms of the ASP116 have the distances of 1.94 and 1.98 Å from the proton of the Schiff base in the resting state model but the distances of 1.78 and 2.11 Å in the KL model. The proton of the Schiff base comes close to one O atom of ASP116 in the KL model. Therefore, it is believed that the proton can move to the ASP116 from the Schiff base in the M intermediate.

**5.3. M Intermediate Model.** In the M model shown in Figure 16c, the hydrogen-bonding distance 1.80 Å between the ASP116 and Schiff base is almost the same as that (1.78 Å) of the KL model. However, since the  $\text{COO}^-$  of ASP116 changes to the  $\text{COOH}$ , the hydrogen-bonding distance between the ASP116 and ASN112 increases to 2.10 Å from 1.83 Å of the KL model. Therefore, the carboxyl group of ASP116 can rotate due to this cavity. The hydrogen-bonding distances between ASN112 and HOH959 and between HOH959 and ASP251 are almost the same as those of the resting and KL models. The blue-shifted M intermediate was calculated to be 3.23 eV that is higher than the experimental value (3.10 eV) by 0.13 eV. This deviation is the same as that of the resting model.

**5.4. R Intermediate Model.** In the R model, by the ASP116 rotation, the new hydrogen bond is formed between the ASP116 and ASN112 as shown in Figure 16d. The distance 3.58 Å between the ASP116 and the Schiff base is longer than that of the M model by 1.78 Å. Therefore, the cavity formed between the Schiff base and ASP116 has enough space for the sodium ion to bind with the Schiff base. Therefore, the sodium ion can move to the cavity from the intracellular medium side and connect with the Schiff base instead of the proton. The excitation energy (3.36 eV) of the R model is slightly higher than that (3.23 eV) of the M model, because the proton of the carboxyl group of the ASP116 is away from the Schiff base.

**5.5. O Intermediate cis Model.** In the  $\text{O0}_{\text{cis}}$  model, the sodium ion moves to the cavity formed by the ASP116 rotation as shown in Figure 17a. The hydrogen-bonding distances

between the ASN112 and HOH959 and between HOH959 and ASP251 hardly change during the photocycle from the resting model to  $\text{O0}_{\text{cis}}$  model. The excitation energy (2.46 eV) of the  $\text{O0}_{\text{cis}}$  model is very close to that (2.49 eV) of the resting model but much lower than those (3.23 and 3.36 eV) of the M and R models, because the Schiff base bonds with the sodium ion instead of the proton.

In the  $\text{O1}_{\text{cis}}$  model shown in Figure 17b, the sodium ion passes through the Schiff base from the intracellular medium side to the

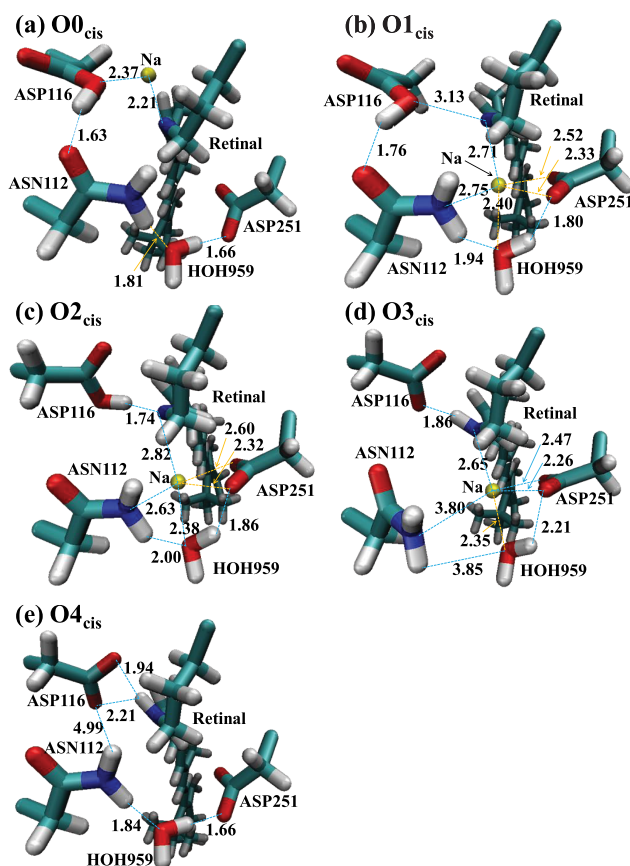


**Figure 17.** Optimized geometries of  $\text{O0}_{\text{cis}}$  (a),  $\text{O1}_{\text{cis}}$  (b),  $\text{O2}_{\text{cis}}$  (c),  $\text{O3}_{\text{cis}}$  (d), and  $\text{O4}_{\text{cis}}$  (e) models of KR2.

extracellular medium side and is surrounded by the Schiff base, ASN112, HOH959 and ASP251. The distance between the Schiff base and the sodium ion increases from 2.21 to 2.71 Å. The hydrogen-bonding distances between ASP116 and ASN112, ASN112 and HOH959, and HOH959 and ASP251 are longer than those of the  $\text{O0}_{\text{cis}}$  model by about 0.13 Å due to the movement of the sodium ion. Since the sodium ion moves away from the Schiff base by 0.50 Å, the excitation energy (2.71 eV) of the  $\text{O1}_{\text{cis}}$  model is higher than that (2.46 eV) of the  $\text{O0}_{\text{cis}}$  model.

In the  $\text{O2}_{\text{cis}}$  model shown in Figure 17c, the sodium ion is surrounded by the Schiff base, ASN112, HOH959 and ASP251 just like the  $\text{O1}_{\text{cis}}$  model and the proton of the carboxyl group of the ASP116 forms the hydrogen bond to the Schiff base by the ASP116 rotation. Therefore, the sodium ion slightly moves from the Schiff base to the HOH959; the distance between the sodium ion and the Schiff base increases to 2.82 Å from 2.71 Å of the  $\text{O1}_{\text{cis}}$  model. The hydrogen-bonding distances between the ASP251 and HOH959 and between ASN112 and HOH959 are

longer than those of the O1<sub>cis</sub> model by about 0.06 Å due to the movement of the sodium ion. The excitation energy (2.56 eV) is lower than that (2.71 eV) of the O1<sub>cis</sub> model, because the sodium ion moves away from the Schiff base but the proton of the carboxyl group of the ASP116 moves toward the Schiff base in comparison to the O1<sub>cis</sub> model.

In the O3<sub>cis</sub> model, since the Schiff base connects with both of the proton and sodium ion as shown in Figure 17d, the geometry optimized calculation was not converged, because two cations binds to the Schiff base. Although the proton reassociates with the Schiff base from the ASP116, the distance between the sodium ion and the Schiff base decreases to 2.65 Å from 2.82 Å of the O2<sub>cis</sub> model. Instead, the distance between the sodium ion and ASN112 increases to 3.80 Å from 2.63 Å of the O2<sub>cis</sub> model due to the rotation of amide group of ASN112. Furthermore, the HOH959 is separated from both the ASN112 and ASP251. Thus, the geometry around the Schiff base is unstable in the O3<sub>cis</sub> model. Since the Schiff base connects with both of the proton and the sodium ion, the excitation energy (1.42 eV) of the O3<sub>cis</sub> model is much lower than those of other models.

In the O4<sub>cis</sub> model, the sodium ion transfers to the extracellular medium. The hydrogen-bonding distances are similar to those of the resting and KL models except for the distance between the ASP116 and ASN112 (Figure 17e). The excitation energy (2.39 eV) of the O4<sub>cis</sub> model is closest to the experimental value (2.19 eV) among the O intermediate models except for the O4'<sub>trans</sub> model.

**5.6. O Intermediate Trans Model.** The optimized geometry of the O1<sub>trans</sub> model is similar to that of the O1<sub>cis</sub> model as shown in Figure 18a. However, the optimized geometries of the other O<sub>trans</sub> models are different from those of the O<sub>cis</sub> models. The carboxylic acid of the ASP116 rotates in the O2<sub>trans</sub> model shown in Figure 18b. The ASN112 rotation occurs in the O3<sub>trans</sub> and O4<sub>trans</sub> models (Figure 18, parts c and d) and the ASP116 rotation occurs in the O4'<sub>trans</sub> model (Figure 18e). Thus, the difference between all-trans and 13-cis of retinal induces the geometrical changes of the amino acids around the Schiff base.

In the optimized geometry of the O1<sub>trans</sub> model, just like in the case of the O1<sub>cis</sub> model, the sodium ion is surrounded by the Schiff base, ASN112, ASP251, and HOH959 as shown in Figure 18a. As can be seen from the retinal structure of each model shown in Figure 19, the retinal structure is distorted around the Schiff base in the O<sub>cis</sub> models but the distortion is decreased in the O<sub>trans</sub> models. Therefore, the excitation energies of the O<sub>trans</sub> models are much higher than the experimental value as well as the SAC-CI values of the O<sub>cis</sub> models. This is similar to the relation between the red-shifted K intermediate with a distorted retinal structure and the blue-shifted L intermediate with a relaxed retinal structure. In the O1<sub>trans</sub> model, the excitation energy (2.95 eV) is much higher than the experimental value (2.19 eV), though the distances of the sodium ion and proton from the Schiff base are closer than those of the O1<sub>cis</sub> model.

The QM/MM optimized calculation was not converged in the O2<sub>trans</sub> model in Figure 18b, unlike in the case of the O2<sub>cis</sub> model. The excitation energy (2.74 eV) is much higher than the experimental value but is slightly lower than that (2.95 eV) of the O1<sub>trans</sub> model, because the distance between the ASP116 and the Schiff base is longer than the hydrogen-bonding distance but shorter than that of the O1<sub>trans</sub> model.

In the O3<sub>trans</sub> model shown in Figure 18c, the Schiff base bonds with both of the proton and sodium ion. The geometry optimized calculation was converged but the ASN112 rotates.

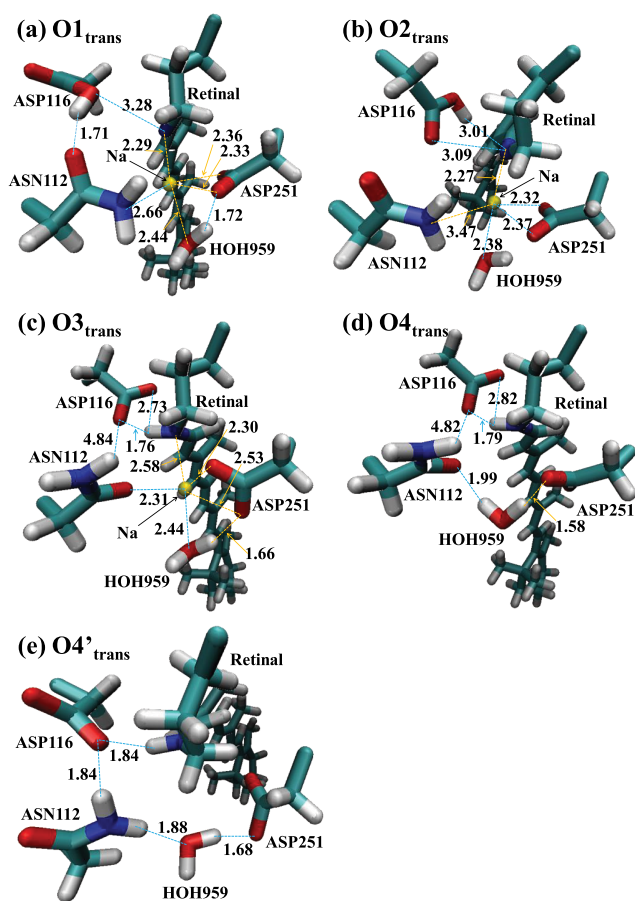


**Figure 18.** Optimized geometries of O1<sub>trans</sub> (a), O2<sub>trans</sub> (b), O3<sub>trans</sub> (c), O4<sub>trans</sub> (d), and O4'<sub>trans</sub> (e) models of KR2.

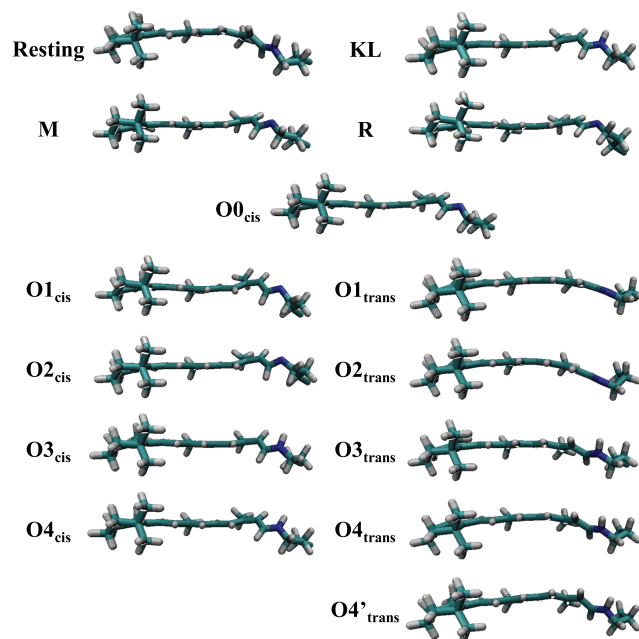


**Figure 19.** Retinal structures of each model of KR2.

Therefore, the obtained geometry is unbelievable. The excitation energy (1.94 eV) of the O3<sub>trans</sub> model is lower than the experimental value due to two cations of the proton and the

sodium ion like the O3<sub>cis</sub> model. Actually, it is difficult for two cations to bind with the Schiff base at the same time like the O3<sub>trans</sub> and O3<sub>cis</sub> models.

In the O4<sub>trans</sub> model in Figure 18d, the sodium ion releases to the extracellular medium. The hydrogen-bonding distances between the Schiff base and the ASP116 and between the ASN112 and ASP116 are similar to those of the O3<sub>trans</sub> model, because the O3<sub>trans</sub> model was used as an initial geometry. The excitation energy (2.85 eV) of the O4<sub>trans</sub> model is higher than that of the O4<sub>cis</sub> model by about 0.5 eV, just like the difference of the excitation energy between the O3<sub>trans</sub> and O3<sub>cis</sub> models.

In the O4'<sub>trans</sub> model in Figure 18e, the O2<sub>trans</sub> model was used as an initial geometry. The obtained geometry is similar to the resting state model except for the rotation of the carboxyl group of ASP116. The difference between the resting state and O4'<sub>trans</sub> models is within 0.02 Å in the hydrogen-bonding distances between ASP116 and ASN112, ASN112 and HOH959, and HOH959 and ASP251. Thus, when the retinal changes from 13-cis to all-trans by the thermal isomerization and the sodium ion moves to the extracellular medium, the geometry of the KR2 can reform to the resting state because the ASP116 easily rotates. The excitation energy (2.19 eV) of the O4'<sub>trans</sub> model is lower than that (2.49 eV) of the resting model, because the hydrogen-bonding distance between the Schiff base and the ASP116 is longer for the O4'<sub>trans</sub> model than that of the resting model due to the ASP116 rotation.

For the O1<sub>trans</sub>, O2<sub>trans</sub>, and O4<sub>trans</sub> models, the excitation energy is much higher than the experimental value. Although the SAC-CI results tend to be higher than the experimental values in other models of KR2, the excitation energy of the O3<sub>trans</sub> model is lower than the experimental value. Therefore, we can conclude that the retinal is not all-trans when the sodium ion passes through the Schiff base.

**5.7. Sodium Ion Pumping Mechanism.** As explained above, the retinal is not all-trans but 13-cis when the sodium ion passes through the Schiff base in the O intermediate. Although the experimental absorption maximum does not change in the O intermediate,<sup>9</sup> the excitation energy is too high for the O1<sub>cis</sub> model and too low for the O3<sub>cis</sub> model, compared with those of the O0<sub>cis</sub>, O2<sub>cis</sub>, and O4<sub>cis</sub> models and the experimental value. If the sodium ion is away from the Schiff base and the proton still remains in the ASP116, the absorption spectrum should be largely blue-shifted like the M intermediate. If the Schiff base bonds to both proton and sodium ion, the absorption spectrum should be largely red-shifted as can be seen from the SAC-CI excitation energy of the O3<sub>cis</sub> model. However, such large blue- or red-shift is not observed in the absorption spectrum of the experimental O intermediate. Therefore, we can suggest that the sodium ion passes through the Schiff base by following three steps. (1) First, the sodium ion bonds with the Schiff base in the cavity between the Schiff base and ASP116 (O0<sub>cis</sub> model). (2) Second, at the same time that the sodium ion passes through the Schiff base and moves to around the ASP251, the proton of ASP116 forms the hydrogen bond to the Schiff base by the ASP116 rotation (O2<sub>cis</sub> model). (3) Finally, the proton of the ASP116 reassociates with the Schiff base at the same time that the sodium ion transfers to the extracellular medium from around the ASP251 (O4<sub>cis</sub> model). From the SAC-CI calculations, the O intermediate in the experiment is considered to correspond to the O4<sub>cis</sub> model, because the excitation energy of only the O4<sub>cis</sub> model is lower than that of the resting state and closest to the experimental value.

## 6. GEOMETRY AND PHOTOCYCLE OF HALORHODOPSIN (HR)

In Table 5, the SAC-CI excitation energies of the resting state and intermediate models are compared with the experimental values<sup>39,98,99</sup> along with the distances between the oxygen atom of the hydroxyl group of SER130 and the nitrogen atom of the Schiff base. The optimized geometries around the Schiff base of the resting, KL, N and O models are explained below.

**6.1. Resting State Model.** In the resting model in Figure 20a, the chloride ion is surrounded by the Schiff base, SER130, THR126, HOH502 and HOH504 that form the hydrogen bonding network along with the HOH503 and ASP252. Therefore, the chloride ion is stabilized by the hydrogen-

**Table 5. Excitation Energies and Distances between the Oxygen Atom of the Hydroxyl Group of the SER130 and the Nitrogen Atom of the Schiff Base of Halorhodopsin (HR)**

model	excitation energy			distance	
	SAC-CI (eV)	exptl (eV)	Δ (eV)	X-ray <sup>d</sup> (Å)	QM/MM <sup>e</sup> (Å)
resting	2.34	2.15 <sup>a</sup> 2.14 <sup>b</sup>	+0.19 +0.20	3.40	3.39
KL	2.34	2.13 (K) <sup>a,f</sup> 2.34 (L) <sup>a,f</sup>	+0.21 0.00	–	4.03
KL <sub>ARG</sub>	2.50	2.13 (K) <sup>a,f</sup> 2.34 (L) <sup>a,f</sup>	+0.37 +0.16	–	4.14
N	2.45	2.14 <sup>a</sup> 2.38 <sup>b</sup> 2.40 <sup>c</sup>	+0.31 +0.05 +0.07	3.73	3.29
O <sub>Org</sub>	1.62	2.07 <sup>a</sup> 2.04 <sup>c</sup>	−0.45 −0.42	3.30	3.63
O <sub>Arg</sub>	1.71	2.07 <sup>a,b</sup> 2.04 <sup>c</sup>	−0.36 −0.33	3.30	3.72
O <sub>OH</sub>	2.19	2.07 <sup>a</sup> 2.04 <sup>c</sup>	+0.12 +0.15	3.30	4.03

<sup>a</sup>Reference 98. <sup>b</sup>Reference 39. <sup>c</sup>Reference 99. <sup>d</sup>Distances in the X-ray crystallographic structures. <sup>e</sup>Distances in the QM/MM optimized geometry. <sup>f</sup>L and K in parentheses represent the experimental values of the L and K intermediates.

bonding interactions. The SAC-CI excitation energy (2.34 eV) is higher than the experimental values by about 0.2 eV. Thus, the SAC-CI values of HR seem to be calculated to be higher than the experimental values in the computational condition used in this article.

**6.2. KL Intermediate Model.** In the KL model in Figure 20b, the chloride ion forms the hydrogen bonds to SER130, THR126, and HOH502. However, the interaction between the chloride ion and the Schiff base becomes weak by the all-trans to 13-cis isomerization. The HOH504 moves close to the ARG123. The THR126 and the SER130 form the hydrogen-bonding network with the ASP252 through the CL, HOH502, and HOH503 by the change of the arrangement of the water molecules. In the optimized geometry, the relaxed retinal structure is close to the L intermediate of BR, but the Schiff base has no hydrogen bond just like the K intermediate of BR. The retinal has the 15-syn conformation for the QM/MM geometry, but 15-anti conformation in the experiment.<sup>36,39</sup> The syn/anti conformational change may occur easily as noted in section 4. In the experiment, the absorption spectrum is slightly red-shifted for the K intermediate but is blue-shifted for the L intermediate.



higher than that of the  $O_{Org}$  model but still lower than the experimental value by more than 0.3 eV.

In the  $O_{OH}$  model, the HOH503 changes to the hydroxide ion with a negative charge. The HOH503 forms the hydrogen bonds to the Schiff base, HOH504, ASP252 and ARG123 as shown in Figure 21c. The THR126 is included in the hydrogen-bonding network by forming the hydrogen bond to the HOH504. In the resting state, the SER130 is an important role to stabilize the chloride ion but is separated from the hydrogen-bonding network in the  $O_{OH}$  model. The SAC-CI excitation energy (2.19 eV) is slightly higher than the experimental values (2.04 and 2.07 eV). Since the SAC-CI values are higher than the experimental values for the resting and N models, this result supports that the HOH503 forming the hydrogen bond to the Schiff base changes to the hydroxide ion instead of the absent chloride ion in the O intermediate.

**6.5. Chloride Ion Pumping Mechanism.** We discuss the chloride ion transfer mechanism in this section. The distances between the oxygen atom of hydroxyl group of the SER130 and the nitrogen atom of the Schiff base are shown in Table 5. In the resting model, the distance between the Schiff base and the SER130 is 3.39 Å. However, the distance is enlarged to 4.03 Å in the KL model. The geometrical change forms the cavity that the chloride ion can pass through the Schiff base. After passing the Schiff base, the distance is reduced to 3.29 Å in the N model. The shortened distance prevents the backflow of chloride ion. This value is shorter than that (3.73 Å) of the X-ray structure by 0.44 Å, because both the Schiff base and the SER130 are attracted to the chloride ion by the QM/MM optimization. In the O models, the distance is enlarged to 3.63, 3.72, and 4.03 Å for the  $O_{Org}$ ,  $O_{Arg}$  and  $O_{OH}$  models. These values are longer than the experimental value (3.30 Å) by about 0.3–0.7 Å, because the Schiff base with a positive charge is attracted by the ASP252 ( $O_{Org}$  and  $O_{Arg}$  models) or the HOH503 ( $O_{OH}$  model) with a negative charge. Since the HOH503 forms the hydrogen bond to the Schiff base in the  $O_{OH}$  model, the distance between the Schiff base and the SER130 is longer than those of the  $O_{Org}$  and  $O_{Arg}$  models.

Figure 7 shows the water molecules included in HR. In the resting state, many water molecules exist in the extracellular medium side of the retinal in Figure 7a. But these water molecules seem to be separated from those in the extracellular medium. However, there are some amino acids with a positive or negative charge between these water molecules. Therefore, a new chloride ion can easily transfer from the extracellular medium to the Schiff base through the water molecule passage. However, only one molecule exists in the intracellular medium side of retinal and there is no amino acid with a positive or negative charge between the retinal and the intracellular medium. Therefore, the chloride ion around the Schiff base cannot transfer to the intracellular medium in the resting state. In short, the chloride ion uptake into the intracellular medium seems not to occur in the resting state.

In the N model in Figure 7b, many water molecules exist between the retinal and the intracellular medium. Therefore, the chloride ion can easily move from the retinal to the intracellular medium through the water molecule passage. Furthermore, though there are also many water molecules between the retinal and the extracellular medium, the chloride ion seems not to move from the extracellular medium to the retinal.

In the O model in Figure 7c, many water molecules disappear from the region between the retinal and the intracellular medium, as in the case of the resting state. This geometrical

change prevents the backflow of the chloride ion from the intracellular medium in the O intermediate. Instead, the chloride ion can move to the Schiff base from the extracellular medium through the water molecule passage so that the HR can return to the resting state.

The chloride ion transfer mechanism is the following: (1) the photoisomerization weakens the hydrogen-bonding interaction between the chloride ion and the Schiff base (KL model), (2) the chloride ion moves from the extracellular medium side to the intracellular medium side of the retinal, keeping the hydrogen bonds to the hydroxyl group of SER130 and the Schiff base (N model), (3) the chloride ion moves to the intracellular medium through the water molecule passage, (4) after the thermal isomerization, the HOH503 bonding to the Schiff base through the hydrogen-bonding interaction changes the hydroxide ion instead of the chloride ion ( $O_{OH}$  model), and (5) the chloride ion moves to the Schiff base from the extracellular medium through the water molecule passage and the hydroxide ion around the Schiff base returns to the water molecule.

## 7. SUMMARY OF ION TRANSFER MECHANISMS OF THREE RHODOPSINS

We summarize and compare three ion transfer mechanisms in this section. For the BR, the SAC-CI results supported the proton transfer mechanism following next six processes: (1) the photoisomerization from the all-trans to 13-cis retinal (K model), (2) the relaxation of the twisted retinal (L model), (3) the proton transfer to ASP85 from the Schiff base (M model), (4) the proton release to the extracellular medium from GLU194 or GLU204 and the proton transfer to the Schiff base from ASP96 (N model), (5) the proton transfer to ASP96 from the intracellular medium and the thermal isomerization to all-trans retinal, and (6) the proton transfer to GLU194 or GLU204 from ASP85 (resting state model). Furthermore, from the comparison between the X-ray and rotation models, the guanidine group rotation of the ARG82 has a large effect on the excitation energies of the L and N intermediates. However, the effect of the guanidine group rotation is limited for the resting state and K, M, and O intermediates. We concluded that the guanidine group of the ARG82 rotates for the N intermediate under the measurement of the experimental absorption spectra from the comparison between the SAC-CI and the experimental values.

The sodium ion transfer mechanism of KR2 is very similar to that of BR from the resting state to the M intermediate. First, the retinal changes from the all-trans to the 13-cis by the photoexcitation in the KL model. Second, the proton transfers from the Schiff base to the counterion residue (ASP116) in the M model. Third, the protonated ASP116 rotates and forms the hydrogen bond to the ASN112 in the R model. Fourth, the sodium ion passes through the Schiff base in the O models. In detail, (1) the sodium ion moves the cavity formed by the ASP116 rotation and connects with the Schiff base ( $O_{O_{cis}}$  model). (2) At the same time that the sodium ion passes through the Schiff base and moves to near the ASP251 from near the ASP116, the ASP116 rotates and forms the hydrogen-bond to the Schiff base ( $O_{2_{cis}}$  model). (3) At the same time that the sodium ion transfers to the extracellular medium, the proton of the ASP116 reassociates with the Schiff base ( $O_{4_{cis}}$  model). In these processes of the O intermediate, the retinal remains the 13-cis. Finally, the KR2 reforms the resting state by the thermal isomerization from the 13-cis retinal to the all-trans retinal.

The chloride ion passing mechanism of HR is slightly different from those of BR and KR2. In the resting state, the chloride ion is stable due to the hydrogen-bonding interactions with the Schiff base, THR126, SER130, HOH502, and HOH504. In the KL model after the photoisomerization, the Schiff base and HOH504 are away from the chloride ion and the cavity is formed between the Schiff base and SER130. The chloride ion passes through the Schiff base from the extracellular medium side to the intracellular medium side in the N model. The retinal conformation changes from the 15-syn to 15-anti before and after the chloride ion passes through the Schiff base. The chloride ion transfers to the intracellular medium through the water molecule passage. In the O<sub>OH</sub> model after the thermal isomerization, the Schiff base forms the hydrogen-bond to the hydroxide ion instead of the chloride ion. In the G, KL and N models, the chloride ion with a negative charge stabilizes the Schiff base with a positive charge. Therefore, the existence of the hydroxide ion with a negative charge is necessary for the stabilization of the Schiff base. Therefore, until a new chloride ion comes to the Schiff base from the extracellular medium, the water molecule forming the hydrogen bond to the Schiff base is considered to become the hydroxide ion.

Thus, the functions are different between three rhodopsins, though all ion transfer reactions start by the photoisomerization of retinal. The main difference between BR and KR2 is that the Schiff base is all-trans for BR but 13-cis for KR2 in the O intermediate. This may be caused by the amino acids and water molecules around the Schiff base. For the BR, the Schiff base forms the hydrogen bond to the water molecule that becomes the part of the hydrogen-bonding network. Therefore, the proton of the Schiff base can move to the extracellular medium through the hydrogen-bonding network formed by the water molecules. However, for the KR2, since there is no water molecule that forms the hydrogen bond to the Schiff base, the proton of the Schiff base moves to the ASP116 in the M intermediate. The proton of the ASP116 can only return to the Schiff base, because only the Schiff base is the acceptor of the proton. Therefore, for the KR2, the retinal is necessary to be 13-cis for the reassociation of the proton with the Schiff base after the sodium ion passes through the Schiff base in the O intermediate. The protonated state is difference between the O intermediate and the resting state for the BR as shown in Table 1, because the Schiff base accepts the proton from the intracellular medium side. However, since the protonated state is the same except for the M and R intermediates for the KR2, the absorption spectral difference may be small between the resting state and O intermediate. Therefore, the O intermediate of KR2 may correspond to the N intermediate of BR.

For the HR, there is no amino acid to receive the proton of the Schiff base. The positive charge always exists in the Schiff base of the retinal during the photocycle. Therefore, only the negative charge can pass through the Schiff base. The photoisomerization to the 13-cis retinal forms (1) the cavity that the chloride ion can pass through the Schiff base (KL model) as well as (2) the water molecule passage that the chloride ion can move from the Schiff base to the intracellular medium (N model in Figure 7b). The thermal isomerization to the all-trans forms the cavity that the chloride ion moves from the extracellular medium to the Schiff base (O model in Figure 7c). The chloride ion moves from the extracellular medium to the intracellular medium through the hydrogen-bonding network formed by the water molecules.

For the BR, the proton of the Schiff base moves to the ASP85 by the all-trans to 13-cis isomerization of retinal. This movement

induces the domino-topping proton transfer reactions. For the KR2, the ASP116 rotation after the photoisomerization of retinal forms the cavity that the sodium ion can pass through the Schiff base. For the HR, The structural change by the photoisomerization of retinal enlarges the distance between the nitrogen atom of the Schiff base and the oxygen atom of hydroxyl group of the SER130. The chloride ion passes through the cavity by the geometrical change of whole protein. Thus, the structural change of the photoisomerization of retinal is a key reaction for three ion-pumping reactions. The light is necessary for the all-trans to 13-cis isomerization that induces these reactions.

## 8. CONCLUSION

We have studied the proton, sodium ion, and chloride ion transfer mechanisms of BR, KR2, and HR by the SAC/SAC-CI calculations using the QM/MM optimized geometries. For the BR, by the initial geometries taken from the X-ray crystallographic structures, the SAC-CI results has reproduced the excitation energies of the resting state and some intermediates and supported the proton transfer mechanism proposed previously. However, for the KR2, since we cannot find all the X-ray crystallographic structures of the intermediates, we calculated the intermediate models constructed from the X-ray crystallographic structure of the resting state. Therefore, our geometries may be different from the actual ones. However, the SAC-CI excitation energies of KR2 showed the reasonable agreement with the experimental values. Therefore, we could support the sodium ion transfer mechanism of KR2 proposed by Kandori group. For HR, the QM/MM optimized geometries are different from the experimental structures for 15-syn/anti conformation of retinal. This may show that 15-syn/anti retinal conformation changes easily. However, from the comparison between the SAC-CI excitation energies and the experimental values, we could suggest the chloride ion transfer mechanism of HR.

The SAC-CI results clarified that for the BR, the rotation of the guanidine group of the ARG82 largely changes the excitation energy for only the L and N intermediates, suggested that for the KR2, the retinal remains 13-cis until the sodium ion passes through the Schiff base in the O intermediate, and suggested that for the HR, the Schiff base forms the hydrogen-bond to the hydroxide ion instead of the chloride ion in the O intermediate. Thus, the SAC-CI method could elucidate the ion transfer mechanism as well as provide the new findings of three rhodopsins.

In this article, we used the LevelTwo, the small QM region and the small basis sets in the SAC-CI calculations. The used monomer model did not include the interaction with the other rhodopsins in trimer and the lipid. These computational conditions are not a high quality. Furthermore, the QM/MM optimized geometries may be local minimum, because they depend on the X-ray crystallographic structures or our constructing models used as the initial geometries. Therefore, the better models and/or the better computation conditions may improve the deviation from the experimental values. However, the present SAC-CI results could support and suggest the ion transfer mechanisms. These findings are important for the elucidation of biological functions and evolutions as well as optogenetic applications. We hope our results will be useful as a guide for elucidating the ion-transfer mechanism, geometries, and functions of new ion-pumping rhodopsins.

## ■ ASSOCIATED CONTENT

### Supporting Information

The Supporting Information is available free of charge on the ACS Publications website at DOI: 10.1021/acs.jpca.8b10203.

Optimized geometries of computational models of BR in PDB format (ZIP)

Optimized geometries of computational models of KR2 in PDB format (ZIP)

Optimized geometries of computational models of HR in PDB format (ZIP)

## ■ AUTHOR INFORMATION

### Corresponding Authors

\*(H.N.) E-mail: [h.nakatsuji@qcri.or.jp](mailto:h.nakatsuji@qcri.or.jp). Telephone: +81-75-634-3211. Fax: +81-75-634-3211.

\*(T.M.) E-mail: [t.miyahara@qcri.or.jp](mailto:t.miyahara@qcri.or.jp).

### ORCID

Tomoo Miyahara: 0000-0002-8683-676X

Hiroshi Nakatsuji: 0000-0002-8162-3220

### Notes

The authors declare no competing financial interest.

## ■ ACKNOWLEDGMENTS

The computations were performed using the computers at the Research Center for Computational Science, Okazaki, Japan, which we acknowledge. We also thank the support of Mr. Nobuo Kawakami for the researches of QCRI. This work was supported by JSPS KAKENHI, Grant Nos. 15K05408, 16H02257 and 17H06233.

## ■ REFERENCES

- (1) Oesterhelt, D.; Stoekenius, W. Rhodopsin-like Protein from the Purple Membrane of Halobacterium halobium. *Nat. New Biol.* **1971**, *233*, 149–152.
- (2) Oesterhelt, D.; Stoekenius, W. Functions of a New Photoreceptor Membrane. *Proc. Natl. Acad. Sci. U. S. A.* **1973**, *70*, 2853–2857.
- (3) Matsuno-Yagi, A.; Mukohata, Y. Two Possible Roles of Bacteriorhodopsin; A Comparative Study of Strains of Halobacterium halobium Differing in Pigmentation. *Biochem. Biophys. Res. Commun.* **1977**, *78*, 237–243.
- (4) Schobert, B.; Lanyi, J. K. Halorhodopsin is a Light-Driven Chloride Pump. *J. Biol. Chem.* **1982**, *257*, 10306–10313.
- (5) Motoyuki, T.; Hazemoto, N.; Kondo, M.; Kamo, N.; Kobatake, Y.; Terayama, Y. Two Photocycles in Halobacterium halobium That Lacks Bacteriorhodopsin. *Biochem. Biophys. Res. Commun.* **1982**, *108*, 970–976.
- (6) Bogomolni, R. A.; Spudich, J. L. Identification of a Third Rhodopsin-like Pigment in Phototactic Halobacterium halobium. *Proc. Natl. Acad. Sci. U. S. A.* **1982**, *79*, 6250–6254.
- (7) Nagel, G.; Ollig, D.; Fuhrmann, M.; Kateriya, S.; Mustl, A. M.; Bamberg, E.; Hegemann, P. Channelrhodopsin-1: A Light-Gated Proton Channel in Green Algae. *Science* **2002**, *296*, 2395–2398.
- (8) Nagel, G.; Szellas, T.; Huhn, W.; Kateriya, S.; Adeishvili, N.; Berthold, P.; Ollig, D.; Hegemann, P.; Bamberg, E. Channelrhodopsin-2, a Directly Light-Gated Cation-Selective Membrane Channel. *Proc. Natl. Acad. Sci. U. S. A.* **2003**, *100*, 13940–13945.
- (9) Inoue, K.; Ono, H.; Abe-Yoshizumi, R.; Yoshizawa, S.; Ito, H.; Kogure, K.; Kandori, H. A Light-Driven Sodium Ion Pump in Marine Bacteria. *Nat. Commun.* **2013**, *4*, 1678.
- (10) Mathies, R. A.; Lin, S. W.; Ames, J. B.; Pollard, W. T. From Femtoseconds to Biology: Mechanism of Bacteriorhodopsin's Light-Driven Proton Pump. *Annu. Rev. Biophys. Biophys. Chem.* **1991**, *20*, 491–518.
- (11) Haupts, U.; Tittor, J.; Oesterhelt, D. Closing in on Bacteriorhodopsin: Progress in Understanding the Molecule. *Annu. Rev. Biophys. Biomol. Struct.* **1999**, *28*, 367–399.
- (12) Kandori, H. Role of Internal Water Molecules in Bacteriorhodopsin. *Biochim. Biophys. Acta, Bioenerg.* **2000**, *1460*, 177–191.
- (13) Váró, G. Analogies between Halorhodopsin and Bacteriorhodopsin. *Biochim. Biophys. Acta, Bioenerg.* **2000**, *1460*, 220–229.
- (14) Balashov, S. P.; Ebrey, T. G. Trapping and Spectroscopic Identification of the Photointermediates of Bacteriorhodopsin at Low Temperatures. *Photochem. Photobiol.* **2001**, *73*, 453–462.
- (15) Herzfeld, J.; Lansing, J. C. Magnetic Resonance Studies of the Bacteriorhodopsin Pump Cycle. *Annu. Rev. Biophys. Biomol. Struct.* **2002**, *31*, 73–95.
- (16) Lanyi, J. K. Bacteriorhodopsin. *Annu. Rev. Physiol.* **2004**, *66*, 665–688.
- (17) Grote, M.; Engelhard, M.; Hegemann, P. Of Ion Pumps, Sensors and Channels - Perspectives on Microbial Rhodopsins Between Science and History. *Biochim. Biophys. Acta, Bioenerg.* **2014**, *1837*, 533–545.
- (18) Gerwert, K.; Freier, E.; Wolf, S. The Role of Protein-Bound Water Molecules in Microbial Rhodopsins. *Biochim. Biophys. Acta, Bioenerg.* **2014**, *1837*, 606–613.
- (19) Inoue, K.; Kato, Y.; Kandori, H. Light-Driven Ion-Translocating Rhodopsins in Marine Bacteria. *Trends Microbiol.* **2015**, *23*, 91–98.
- (20) Wickstrand, C.; Dods, R.; Royant, A.; Neutze, R. Bacteriorhodopsin: Would the Real Structural Intermediates Please Stand Up? *Biochim. Biophys. Acta, Gen. Subj.* **2015**, *1850*, 536–553.
- (21) Govorunova, E. G.; Sineshchekov, O. A.; Li, H.; Spudich, J. L. Microbial Rhodopsins: Diversity, Mechanisms, and Optogenetic Applications. *Annu. Rev. Biochem.* **2017**, *86*, 845–872.
- (22) Brown, L. S.; Ernst, O. P. Recent Advances in Biophysical Studies of Rhodopsins - Oligomerization, Folding, and Structure. *Biochim. Biophys. Acta, Proteins Proteomics* **2017**, *1865*, 1512–1521.
- (23) Váró, G.; Lanyi, J. K. Kinetic and Spectroscopic Evidence for an Irreversible Step Between Deprotonation and Reprotonation of the Schiff Base in the Bacteriorhodopsin Photocycle. *Biochemistry* **1991**, *30*, 5008–5015.
- (24) Kato, H. E.; Inoue, K.; Abe-Yoshizumi, R.; Kato, Y.; Ono, H.; Konno, M.; Hososhima, S.; Ishizuka, T.; Hoque, M. R.; Kunitomo, H.; Ito, J.; Yoshizawa, S.; Yamashita, K.; Takemoto, M.; Nishizawa, T.; Taniguchi, R.; Kogure, K.; Maturana, A. D.; Iino, Y.; Yawo, H.; Ishitani, R.; Kandori, H.; Nureki, O. Structural Basis for Na<sup>+</sup> Transport Mechanism by a Light-Driven Na<sup>+</sup> Pump. *Nature* **2015**, *521*, 48–53.
- (25) Abe-Yoshizumi, R.; Inoue, K.; Kato, H. E.; Nureki, O.; Kandori, H. Role of Asn112 in a Light-Driven Sodium Ion-Pumping Rhodopsin. *Biochemistry* **2016**, *55*, 5790–5797.
- (26) Suomivuori, C.-M.; Gamiz-Hernandez, A. P.; Sundholm, D.; Kaila, V. R. I. Energetics and Dynamics of a Light-Driven Sodium-Pumping Rhodopsin. *Proc. Natl. Acad. Sci. U. S. A.* **2017**, *114*, 7043–7048.
- (27) Balashov, S. P.; Imasheva, E. S.; Dioumaev, A. K.; Wang, J. M.; Jung, K.-H.; Lanyi, J. K. Light-Driven Na<sup>+</sup> Pump from *Gillisia limnaea*: A High-Affinity Na<sup>+</sup> Binding Site Is Formed Transiently in the Photocycle. *Biochemistry* **2014**, *53*, 7549–7561.
- (28) Ono, H.; Inoue, K.; Abe-Yoshizumi, R.; Kandori, H. FTIR Spectroscopy of a Light-Driven Compatible Sodium Ion-Proton Pumping Rhodopsin at 77 K. *J. Phys. Chem. B* **2014**, *118*, 4784–4792.
- (29) Tahara, S.; Takeuchi, S.; Abe-Yoshizumi, R.; Inoue, K.; Ohtani, H.; Kandori, H.; Tahara, T. Ultrafast Photochemical Dynamics of a Light-Driven Sodium-Ion-Pumping Retinal Protein from *Krokinobacter eikastus* Revealed by Femtosecond Time-Resolved Absorption Spectroscopy. *J. Phys. Chem. Lett.* **2015**, *6*, 4481–4486.
- (30) Gushchin, I.; Shevchenko, V.; Polovinkin, V.; Borshchevskiy, V.; Buslaev, P.; Bamberg, E.; Gordeliy, V. Structure of the Light-Driven Sodium Pump KR2 and Its Implications for Optogenetics. *FEBS J.* **2016**, *283*, 1232–1238.
- (31) Bogachev, A. V.; Bertsova, Y. V.; Verkhovskaya, M. L.; Mamedov, M. D.; Skulachev, V. P. Real-Time Kinetics of Electrogenic Na<sup>+</sup> Transport by Rhodopsin from the Marine Flavobacterium *Dokdonia* sp. Pro95. *Sci. Rep.* **2016**, *6*, 21397.

- (32) Kato, H. E.; Inoue, K.; Kandori, H.; Nureki, O. The Light-Driven Sodium Ion Pump: A New Player in Rhodopsin Research. *BioEssays* **2016**, *38*, 1274–1282.
- (33) Hontani, Y.; Inoue, K.; Kloz, M.; Kato, Y.; Kandori, H.; Kennis, J. T. M. The Photochemistry of Sodium Ion Pump Rhodopsin Observed by Watermarked Femto- to Submillisecond Stimulated Raman Spectroscopy. *Phys. Chem. Chem. Phys.* **2016**, *18*, 24729–24736.
- (34) Kajimoto, K.; Kikukawa, T.; Nakashima, H.; Yamaryo, H.; Saito, Y.; Fujisawa, T.; Demura, M.; Unno, M. Transient Resonance Raman Spectroscopy of a Light-Driven Sodium-Ion-Pump Rhodopsin from *Indibacter alkaliphilus*. *J. Phys. Chem. B* **2017**, *121*, 4431–4437.
- (35) Zhao, H.; Ma, B.; Ji, L.; Li, L.; Wang, H.; Chen, D. Coexistence of Light-Driven Na<sup>+</sup> and H<sup>+</sup> Transport in a Microbial Rhodopsin from *Nonlabens dokdonensis*. *J. Photochem. Photobiol., B* **2017**, *172*, 70–76.
- (36) Essen, L.-O. Halorhodopsin: Light-Driven Ion Pumping Made Simple? *Curr. Opin. Struct. Biol.* **2002**, *12*, 516–522.
- (37) Ernst, O. P.; Lodowski, D. T.; Elstner, M.; Hegemann, P.; Brown, L. S.; Kandori, H. Microbial and Animal Rhodopsins: Structures, Functions, and Molecular Mechanisms. *Chem. Rev.* **2014**, *114*, 126–163.
- (38) Gmelin, W.; Zeth, K.; Efremov, R.; Heberle, J.; Tittor, J.; Oesterheld, D. The Crystal Structure of the L1 Intermediate of Halorhodopsin at 1.9 Å Resolution. *Photochem. Photobiol.* **2007**, *83*, 369–377.
- (39) Kouyama, T.; Kawaguchi, H.; Nakanishi, T.; Kubo, H.; Murakami, M. Crystal Structures of the L1, L2, N, and O States of pharaonis Halorhodopsin. *Biophys. J.* **2015**, *108*, 2680–2690.
- (40) Shichida, Y.; Matsuyama, T. Evolution of Opsins and Phototransduction. *Philos. Trans. R. Soc., B* **2009**, *364*, 2881–2895.
- (41) Nakatsuji, H.; Hirao, K. Cluster Expansion of the Wavefunction. Symmetry-Adapted-Cluster Expansion, Its Variational Determination, and Extension of Open-Shell Orbital Theory. *J. Chem. Phys.* **1978**, *68*, 2053–2065.
- (42) Nakatsuji, H. Cluster Expansion of the Wavefunction. Excited States. *Chem. Phys. Lett.* **1978**, *59*, 362–364.
- (43) Nakatsuji, H. Cluster Expansion of the Wavefunction. Electron Correlations in Ground and Excited States by SAC (Symmetry-Adapted-Cluster) and SAC-CI Theories. *Chem. Phys. Lett.* **1979**, *67*, 329–333.
- (44) Nakatsuji, H. Cluster Expansion of the Wavefunction. Calculation of Electron Correlations in Ground and Excited States by SAC and SAC-CI Theories. *Chem. Phys. Lett.* **1979**, *67*, 334–342.
- (45) Fujimoto, K.; Hasegawa, J.; Hayashi, S.; Kato, S.; Nakatsuji, H. Mechanism of Color Tuning in Retinal Protein: SAC-CI and QM/MM Study. *Chem. Phys. Lett.* **2005**, *414*, 239–242.
- (46) Fujimoto, K.; Hasegawa, J.; Hayashi, S.; Nakatsuji, H. On the Color-Tuning Mechanism of Human-Blue Visual Pigment: SAC-CI and QM/MM Study. *Chem. Phys. Lett.* **2006**, *432*, 252–256.
- (47) Fujimoto, K.; Hayashi, S.; Hasegawa, J.; Nakatsuji, H. Theoretical Studies on the Color-Tuning Mechanism in Retinal Proteins. *J. Chem. Theory Comput.* **2007**, *3*, 605–618.
- (48) Fujimoto, K.; Hasegawa, J.; Nakatsuji, H. Origin of Color Turning in Human Red, Green, and Blue Cone Pigments: SAC-CI and QM/MM Study. *Chem. Phys. Lett.* **2008**, *462*, 318–320.
- (49) Fujimoto, K.; Hasegawa, J.; Nakatsuji, H. Color Tuning Mechanism of Human Red, Green, and Blue Cone Pigments: SAC-CI Theoretical Study. *Bull. Chem. Soc. Jpn.* **2009**, *82*, 1140–1148.
- (50) Nakatsuji, H. Electronic Structures of Ground, Excited, Ionized, and Anion States Studied by the SAC/SAC-CI Theory. *Acta Chimica Hungarica Models in Chemistry* **1992**, *129*, 719–776.
- (51) Nakatsuji, H. SAC-CI Method: Theoretical Aspects and Some Recent Topics. *Computational Chemistry: Reviews of Current Trends* **1997**, *2*, 62–124.
- (52) Ehara, M.; Hasegawa, J.; Nakatsuji, H. SAC-CI Method Applied to Molecular Spectroscopy. *Theory and Applications of Computational Chemistry: The First 40 Years, A Volume of Technical and Historical Perspectives* **2005**, 1099–1141.
- (53) Hasegawa, J.; Nakatsuji, H. Exploring Photo-Biology and Bio-Spectroscopy with the SAC-CI (Symmetry-Adapted Cluster-Configuration Interaction) Method. *Radiation Induced Molecular Phenomena in Nucleic Acid: A Comprehensive Theoretical and Experimental Analysis* **2008**, *5*, 93–124.
- (54) Miyahara, T.; Nakatsuji, H. Circular Dichroism Spectroscopy with the SAC-CI Methodology: A ChiraSac Study. *Frontiers of Quantum Chemistry* **2018**, 21–47.
- (55) Nakatsuji, H.; Hasegawa, J.; Ohkawa, K. Excited States and Electron Transfer Mechanism in the Photosynthetic Reaction Center of *Rhodospseudomonas Viridis*: SAC-CI Study. *Chem. Phys. Lett.* **1998**, *296*, 499–504.
- (56) Hasegawa, J.; Ohkawa, K.; Nakatsuji, H. Excited States of the Photosynthetic Reaction Center of *Rhodospseudomonas Viridis*: SAC-CI Study. *J. Phys. Chem. B* **1998**, *102*, 10410–10419.
- (57) Hasegawa, J.; Nakatsuji, H. Mechanism and Unidirectionality of the Electron Transfer in the Photosynthetic Reaction Center of *Rhodospseudomonas Viridis*: SAC-CI Theoretical Study. *J. Phys. Chem. B* **1998**, *102*, 10420–10430.
- (58) Ito, H.; Nakatsuji, H. Roles of Proteins in the Electron Transfer in the Photosynthetic Reaction Center of *Rhodospseudomonas Viridis*: Bacteriopheophytin to Ubiquinone. *J. Comput. Chem.* **2001**, *22*, 265–272.
- (59) Ohtsuka, Y.; Ohkawa, K.; Nakatsuji, H. Electron Transfer in the C-Type Cytochrome Subunit of the Photosynthetic Reaction Center of *Rhodospseudomonas Viridis*: Ab Initio Theoretical Study. *J. Comput. Chem.* **2001**, *22*, 521–527.
- (60) Ohkawa, K.; Hada, M.; Nakatsuji, H. Excited States of Four Hemes in a C-Type Cytochrome Subunit of the Photosynthetic Reaction Center of *Rhodospseudomonas Viridis*: SAC-CI Calculations. *J. Porphyrins Phthalocyanines* **2001**, *5*, 256–266.
- (61) Hasegawa, J.; Ishida, M.; Nakatsuji, H.; et al. Energetics of the Electron Transfer from Bacteriopheophytin to Ubiquinone in the Photosynthetic Reaction Center of *Rhodospseudomonas Viridis*: Theoretical Study. *J. Phys. Chem. B* **2003**, *107*, 838–847.
- (62) Das, A. K.; Hasegawa, J.; Miyahara, T.; Ehara, M.; Nakatsuji, H. Electronic Excitations of the Green Fluorescent Protein Chromophore in Its Protonation States: SAC/SAC-CI Study. *J. Comput. Chem.* **2003**, *24*, 1421–1431.
- (63) Hasegawa, J.; Fujimoto, K.; Swerts, B.; Miyahara, T.; Nakatsuji, H. Excited States of GFP Chromophore and Active Site Studied by the SAC-CI method: Effect of Protein-Environment and Mutations. *J. Comput. Chem.* **2007**, *28*, 2443–2452.
- (64) Nakatani, N.; Hasegawa, J.; Nakatsuji, H. Red Light in Chemiluminescence and Yellow-Green Light in Bioluminescence: Color-Tuning Mechanism of Firefly, *Photinus pyralis*, Studied by the Symmetry-Adapted Cluster-Configuration Interaction Method. *J. Am. Chem. Soc.* **2007**, *129*, 8756–8765.
- (65) Nakatani, N.; Hasegawa, J.; Nakatsuji, H. Artificial Color Tuning of Firefly Luminescence: Theoretical Mutation by Tuning Electrostatic Interactions Between Protein and Luciferin. *Chem. Phys. Lett.* **2009**, *469*, 191–194.
- (66) Miyahara, T.; Nakatsuji, H.; Sugiyama, H. Helical Structure and Circular Dichroism Spectra of DNA: A Theoretical Study. *J. Phys. Chem. A* **2013**, *117*, 42–55.
- (67) Miyahara, T.; Nakatsuji, H.; Wada, T. Circular Dichroism Spectra of Uridine Derivatives: ChiraSac Study. *J. Phys. Chem. A* **2014**, *118*, 2931–2941.
- (68) Miyahara, T.; Nakatsuji, H. Indicator of the Stacking Interaction in the DNA Double-Helical Structure: ChiraSac Study. *J. Phys. Chem. A* **2015**, *119*, 8269–8278.
- (69) Miyahara, T.; Nakatsuji, H.; Sugiyama, H. Similarities and Differences between RNA and DNA Double-Helical Structures in Circular Dichroism Spectroscopy: A SAC-CI Study. *J. Phys. Chem. A* **2016**, *120*, 9008–9018.
- (70) Casida, M. E. Time-Dependent Density Functional Response Theory for Molecules. *Recent Advances in Density Functional Methods Part I (Recent Advances in Computational Chemistry)* **1995**, *1*, 155–192.
- (71) Bauernschmitt, R.; Ahlrichs, R. Treatment of Electronic Excitations Within the Adiabatic Approximation of Time Dependent Density Functional Theory. *Chem. Phys. Lett.* **1996**, *256*, 454–464.

- (72) Stratmann, R. E.; Scuseria, G. E.; Frisch, M. J. An Efficient Implementation of Time-Dependent Density-Functional Theory for the Calculation of Excitation Energies of Large Molecules. *J. Chem. Phys.* **1998**, *109*, 8218–8224.
- (73) Leang, S. S.; Zahariev, F.; Gordon, M. S. Benchmarking the Performance of Time-Dependent Density Functional Methods. *J. Chem. Phys.* **2012**, *136*, 104101–1–12.
- (74) Isegawa, M.; Peverati, R.; Truhlar, D. G. Performance of Recent and High-Performance Approximate Density Functionals for Time-Dependent Density Functional Theory Calculations of Valence and Rydberg Electronic Transition Energies. *J. Chem. Phys.* **2012**, *137*, 244104–1–17.
- (75) Laurent, A. D.; Jacquemin, D. TD-DFT Benchmarks: A Review. *Int. J. Quantum Chem.* **2013**, *113*, 2019–2039.
- (76) Mardirossian, N.; Head-Gordon, M.  $\omega$ B97X-V: A 10-Parameter, Range-Separated Hybrid, Generalized Gradient Approximation Density Functional with Nonlocal Correlation, Designed by a Survival-of-the-Fittest Strategy. *Phys. Chem. Chem. Phys.* **2014**, *16*, 9904–9924.
- (77) Luecke, H.; Schobert, B.; Richter, H.-T.; Cartailier, J.-P.; Lanyi, J. K. Structure of Bacteriorhodopsin at 1.55 Å Resolution. *J. Mol. Biol.* **1999**, *291*, 899–911.
- (78) Schobert, B.; Cupp-Vickery, J.; Hornak, V.; Smith, S. O.; Lanyi, J. K. Crystallographic Structure of the K Intermediate of Bacteriorhodopsin: Conservation of Free Energy After Photoisomerization of the Retinal. *J. Mol. Biol.* **2002**, *321*, 715–726.
- (79) Lanyi, J. K.; Schobert, B. Mechanism of Proton Transport in Bacteriorhodopsin from Crystallographic Structures of the K, L, M1, M2, and M2' Intermediates of the Photocycle. *J. Mol. Biol.* **2003**, *328*, 439–450.
- (80) Schobert, B.; Brown, L. S.; Lanyi, J. K. Crystallographic Structures of the M and N Intermediates of Bacteriorhodopsin: Assembly of a Hydrogen-Bonded Chain of Water Molecules Between Asp-96 and the Retinal Schiff Base. *J. Mol. Biol.* **2003**, *330*, 553–570.
- (81) Zhang, J.; Yamazaki, Y.; Hikake, M.; Murakami, M.; Ihara, K.; Kouyama, T. Crystal Structure of the O Intermediate of the Leu93→Ala Mutant of Bacteriorhodopsin. *Proteins: Struct., Funct., Genet.* **2012**, *80*, 2384–2396.
- (82) Kouyama, T.; Kanada, S.; Takeguchi, Y.; Narusawa, A.; Murakami, M.; Ihara, K. Crystal Structure of the Light-Driven Chloride Pump Halorhodopsin from *Natronomonas pharaonis*. *J. Mol. Biol.* **2010**, *396*, 564–579.
- (83) Kanada, S.; Takeguchi, Y.; Murakami, M.; Ihara, K.; Kouyama, T. Crystal Structures of an O-Like Blue Form and an Anion-Free Yellow Form of *pharaonis* Halorhodopsin. *J. Mol. Biol.* **2011**, *413*, 162–176.
- (84) Ponder, J. W. *TINKER: Software Tools for Molecular Design*, 7.0 ed.; 2014.
- (85) Wang, J.; Cieplak, P.; Kollman, P. A. How Well Does a Restrained Electrostatic Potential (RESP) Model Perform in Calculating Conformational Energies of Organic and Biological Molecules? *J. Comput. Chem.* **2000**, *21*, 1049–1074.
- (86) Dennington, R.; Keith, T. A.; Millam, J. M., *GaussView*, Version 5; Semichem Inc.: Shawnee Mission, KS, 2009.
- (87) Parr, R. G.; Yang, W.; *Density-Functional Theory of Atoms and Molecules*; Oxford University Press: Oxford, U.K., 1989.
- (88) Becke, A. D. Density-Functional Thermochemistry. III. The Role of Exact Exchange. *J. Chem. Phys.* **1993**, *98*, 5648–5652.
- (89) Lee, C.; Yang, W.; Parr, R. G. Development of the Colle-Salvetti Correlation-Energy Formula into a Functional of the Electron Density. *Phys. Rev. B: Condens. Matter Mater. Phys.* **1988**, *37*, 785–789.
- (90) Hariharan, P. C.; Pople, J. A. The Influence of Polarization Functions on Molecular Orbital Hydrogenation Energies. *Theoret. Chim. Acta* **1973**, *28*, 213–222.
- (91) Humphrey, W.; Dalke, A.; Schulten, K. VMD: Visual Molecular Dynamics. *J. Mol. Graphics* **1996**, *14*, 33–38.
- (92) Frisch, M. J.; Trucks, G. W.; Schlegel, H. B.; Scuseria, G. E.; Robb, M. A.; Cheeseman, J. R.; Scalmani, G.; Barone, V.; Petersson, G. A.; Nakatsuji, H.; Li, X.; Caricato, M.; Marenich, A. V.; Bloino, J.; Janesko, B. G.; Gomperts, R.; Mennucci, B.; Hratchian, H. P.; Ortiz, J. V.; Izmaylov, A. F.; Sonnenberg, J. L.; Williams-Young, D.; Ding, F.; Lipparini, F.; Egidi, F.; Goings, J.; Peng, B.; Petrone, A.; Henderson, T.; Ranasinghe, D.; Zakrzewski, V. G.; Gao, J.; Rega, N.; Zheng, G.; Liang, W.; Hada, M.; Ehara, M.; Toyota, K.; Fukuda, R.; Hasegawa, J.; Ishida, M.; Nakajima, T.; Honda, Y.; Kitao, O.; Nakai, H.; Vreven, T.; Throssell, K.; Montgomery, J. A., Jr.; Peralta, J. E.; Ogliaro, F.; Bearpark, M. J.; Heyd, J. J.; Brothers, E. N.; Kudin, K. N.; Staroverov, V. N.; Keith, T. A.; Kobayashi, R.; Normand, J.; Raghavachari, K.; Rendell, A. P.; Burant, J. C.; Iyengar, S. S.; Tomasi, J.; Cossi, M.; Millam, J. M.; Klene, M.; Adamo, C.; Cammi, R.; Ochterski, J. W.; Martin, R. L.; Morokuma, K.; Farkas, O.; Foresman, J. B.; Fox, D. J. *Gaussian 09: Gaussian, Inc.: Wallingford CT*, 2009.
- (93) Dunning, T. H.; Hay, P. J. Gaussian Basis Sets for Molecular Calculations. *Modern Theoretical Chemistry* **1977**, *3*, 1–27.
- (94) Canal Neto, A.; Muniz, E. P.; Centoducatte, R.; Jorge, F. E. Gaussian Basis Sets for Correlated Wave Functions. Hydrogen, Helium, First- and Second-Row Atoms. *J. Mol. Struct.: THEOCHEM* **2005**, *718*, 219–224.
- (95) Nakatsuji, H. Cluster Expansion of the Wavefunction. Valence and Rydberg Excitations, Ionizations, and Inner-Valence Ionizations of CO<sub>2</sub> and N<sub>2</sub>O Studied by the SAC and SAC-CI Theories. *Chem. Phys.* **1983**, *75*, 425–441.
- (96) Kouyama, T.; Nishikawa, T.; Tokuhisa, T.; Okumura, H. Crystal Structure of the L Intermediate of Bacteriorhodopsin: Evidence for Vertical Translocation of a Water Molecule During the Proton Pumping Cycle. *J. Mol. Biol.* **2004**, *335*, 531–546.
- (97) Takeda, K.; Matsui, Y.; Kamiya, N.; Adachi, S.; Okumura, H.; Kouyama, T. Crystal Structure of the M Intermediate of Bacteriorhodopsin: Allosteric Structural Changes Mediated by Sliding Movement of a Transmembrane Helix. *J. Mol. Biol.* **2004**, *341*, 1023–1037.
- (98) Váró, G.; Brown, L. S.; Sasaki, J.; Kandori, H.; Maeda, A.; Needleman, R.; Lanyi, J. K. Light-Driven Chloride Ion Transport by Halorhodopsin from *Natronobacterium pharaonis*. 1. The Photochemical Cycle. *Biochemistry* **1995**, *34*, 14490–14499.
- (99) Shibasaki, K.; Shigemura, H.; Kikukawa, T.; Kamiya, M.; Aizawa, T.; Kawano, K.; Kamo, N.; Demura, M. Role of Thr218 in the Light-Driven Anion Pump Halorhodopsin from *Natronomonas pharaonis*. *Biochemistry* **2013**, *52*, 9257–9268.